



INSTITUT DE FRANCE  
Académie des sciences

# *Comptes Rendus*

---

## *Géoscience*

### *Sciences de la Planète*

Marc Poujol, Mathilde Mercuzot, Michel Lopez, Sylvie Bourquin, Olivier Bruguier, Erwan Hallot and Laurent Beccaletto

**Insights on the Permian tuff beds from the Saint-Affrique Basin (Massif Central, France): an integrated geochemical and geochronological study**

Volume 355, Special Issue S2 (2023), p. 137-161


Online since: 20 January 2023

Issue date: 23 February 2024

**Part of Special Issue:** Tribute to Jean Dercourt

**Guest editors:** François Baudin (Institut des Sciences de la Terre - Paris (ISTeP), Sorbonne Université), Éric Calais (École normale supérieure, Département de Géosciences, Paris) and François Chabaux (Institut Terre Environnement de Strasbourg (UMR 7063-Unistra-CNRS-ENGEES), Université de Strasbourg)

<https://doi.org/10.5802/crgeos.184>

 This article is licensed under the  
CREATIVE COMMONS ATTRIBUTION 4.0 INTERNATIONAL LICENSE.  
<http://creativecommons.org/licenses/by/4.0/>



*The Comptes Rendus. Géoscience — Sciences de la Planète are a member of the  
Mersenne Center for open scientific publishing*

[www.centre-mersenne.org](http://www.centre-mersenne.org) — e-ISSN : 1778-7025



---

Research article

Tribute to Jean Dercourt

# Insights on the Permian tuff beds from the Saint-Affrique Basin (Massif Central, France): an integrated geochemical and geochronological study

Marc Poujol<sup>Ⓣ,\* ,a</sup>, Mathilde Mercuzot<sup>Ⓣ,a</sup>, Michel Lopez<sup>Ⓣ,b</sup>, Sylvie Bourquin<sup>Ⓣ,a</sup>, Olivier Bruguier<sup>Ⓣ,b</sup>, Erwan Hallot<sup>Ⓣ,a</sup> and Laurent Beccaletto<sup>Ⓣ,c</sup>

<sup>a</sup> Univ. Rennes, CNRS, Géosciences Rennes, UMR6118, F-35000 Rennes, France

<sup>b</sup> Géosciences Montpellier, Université de Montpellier, CNRS, F-34000 Montpellier, France

<sup>c</sup> BRGM, F-45060 Orléans, France

*E-mails:* marc.poujol@univ-rennes1.fr (M. Poujol), mathilde.mercuzot@outlook.com (M. Mercuzot), michel.lopez@umontpellier.fr (M. Lopez), sylvie.bourquin@univ-rennes1.fr (S. Bourquin), Olivier.Bruguier@gm.univ-montp2.fr (O. Bruguier), erwan.hallot@univ-rennes1.fr (E. Hallot), l.beccaletto@brgm.fr (L. Beccaletto)

**Abstract.** The Permian marks the transition between the end of the accretion of the supercontinent Pangea and the beginning of its dislocation. In the Eastern Pangea intertropical domain (i.e. the present-day Western Europe), the late-Paleozoic (i.e. uppermost Carboniferous–Permian) history remains poorly constrained due to the lack of precise radiometric data. This is particularly true for Permian basins from the southern part of the French Massif Central, making it difficult to determine correlations between basins and therefore robust timings and constraints on the environmental and climate events described in these basins, and to compare them with the larger-scale settings. This article focuses on the Saint-Affrique Basin, via an integrated petrological, geochemical and geochronological study of eight of the volcanic-ash levels interbedded in the sedimentary succession. It highlights the existence of two different groups of felsic volcanoclastic rocks. The first group, located at the base of the basin and attributed to the Stephanian continental stage, is related to a late-orogenic volcanic setting and corresponds to calc-alkaline trachy-andesitic tuffites that could not be dated due to the lack of volcanic zircon. The second group, located towards the top of the succession, is composed of calc-alkaline dacitic ash beds and tuffites yielding Kungurian ages, i.e. late early Permian (Cisuralian,  $283.5 \pm 0.6$  to  $273.01 \pm 0.14$  Ma), and are attributed to a post-orogenic deposition setting. These ages show that the sedimentary filling of the basin is younger than hitherto expected (i.e. Artinskian,  $290.1 \pm 0.26$  to  $283.5 \pm 0.6$  Ma). The elemental geochemistry, the presence of inherited detrital zircons and the Hf signatures of the volcanic ones indicate the involvement of an

---

\* Corresponding author.

old (Proterozoic and older) basement in the magma genesis; this crustal contribution becomes more prominent towards the top of the sedimentary succession.

**Keywords.** Continental Permian basin, Zircon, LA-ICP-MS dating, Volcanism, French Massif Central.

*Manuscript received 23 July 2022, revised 31 October 2022, accepted 15 November 2022.*

## 1. Introduction

The Permian marks the transition between the end of the accretion of the supercontinent Pangea and the beginning of its dislocation [e.g. Scotese and Langford, 1995, Stampfli and Kozur, 2006, Stampfli *et al.*, 2013, Domeier and Torsvik, 2014]. From the end of the Carboniferous onwards, the Variscan belt, still in erosion, experienced a gravitational collapse [Ménard and Molnar, 1988, Malavieille *et al.*, 1990, Van Den Driessche and Brun, 1992, Burg *et al.*, 1994, Faure, 1995]. The eastern Pangea intra-mountain domain then underwent a generalized extension that resulted in the formation of extensive structures and rifts forming narrow continental basins at the end of the Carboniferous, which widened during the Permian [Ménard and Molnar, 1988, Vallé *et al.*, 1988, Van Den Driessche and Brun, 1989, 1992, Burg *et al.*, 1990, Malavieille *et al.*, 1990, Faure and Becq-Giraudon, 1993, Faure, 1995, Becq-Giraudon *et al.*, 1996, Genna *et al.*, 1998, Choulet *et al.*, 2012, Beccaletto *et al.*, 2015]. This late-to-post-Variscan transition was widely accompanied by aerial volcanism which has been well recorded in numerous continental siliciclastic sedimentary basins, either as a volcanogenic fraction in the sediments, or as inter-layered volcanic ash beds that are still mostly undated [Odin and Conrad, 1987, Châteauneuf and Farjanel, 1989, Nmila, 1995, Timmerman, 2004, Pellenard *et al.*, 2017, Ducassou *et al.*, 2019].

Due to the lack of precise radiometric data and marine biostratigraphic markers, the timings of the late Paleozoic (i.e. uppermost Carboniferous–Permian) history remains poorly constrained in the Eastern Pangea intertropical domain (i.e. the present-day western European basins). This is therefore problematic to accurately reconstruct the paleogeography and the evolution of the depositional environments. The current stratigraphic framework implies a nomenclature specific to European continental basins, with a terminology based on lithology as well as on the floristic and ichnological content [Izart *et al.*, 1998, Lucas and Shen, 2018, Schneider *et al.*, 2020]. Thus, the most recent late-Paleozoic paleogeographic reconstructions incorporate the

Middle to Upper Permian series without distinction. In addition, it is not currently possible to provide a paleogeographic outline of the Lower Permian basins for the terrestrial domain [e.g. Bourquin *et al.*, 2011]. Moreover, new age constraints on the sedimentary successions will allow to accurately link the observed environmental and climate perturbations recorded in the sedimentary successions [e.g. Mercuzot *et al.*, 2021] to the global climate dynamics.

Significant advances have been recently obtained in terms of temporal calibration (dating of volcanogenic levels) and depositional environments of the Carboniferous–Permian finite age series of the northern Massif Central [Pellenard *et al.*, 2017, Ducassou *et al.*, 2019, Mercuzot. *et al.*, 2021, Mercuzot *et al.*, 2021, 2022].

In contrast, little is known about the age and nature of the volcanism in the Carboniferous–Permian basins from south of the Massif Central (Saint-Affrique, Lodève-Graissessac and Gabian-Neffiès basins), where only a few volcanogenic layers in the Lodève-Graissessac Basin have been dated so far [e.g. Bruguier *et al.*, 2003, Michel *et al.*, 2015]. However, numerous volcanic ash beds have been described [Goloubinoff, 1979, Rolando, 1988], in particular thanks to the discovery of uranium mineralization in 1957 in the Lodève Basin during a radio-prospecting campaign performed by the French atomic energy commission (i.e. CEA, Commissariat à l’Energie Atomique). Nearly 240 wells were then drilled and twenty-four different ash beds were identified and numbered using Roman numerals (I to XXIV), following the order of discovery and consequently not the stratigraphic order. Once these benchmark levels had been described and identified in the Lodève Basin, uranium prospectors then mapped the Saint-Affrique Basin (Figure 1A) in order to look for potential sister uranium deposits. There, they also identified several volcanic ash beds and established correlations with those described in the Lodève Basin based on their facies architecture [e.g. Hübner *et al.*, 2011]. These volcanic ash beds have not been dated yet, nor characterized geochemically. Therefore, the aim of this study is to provide new information on

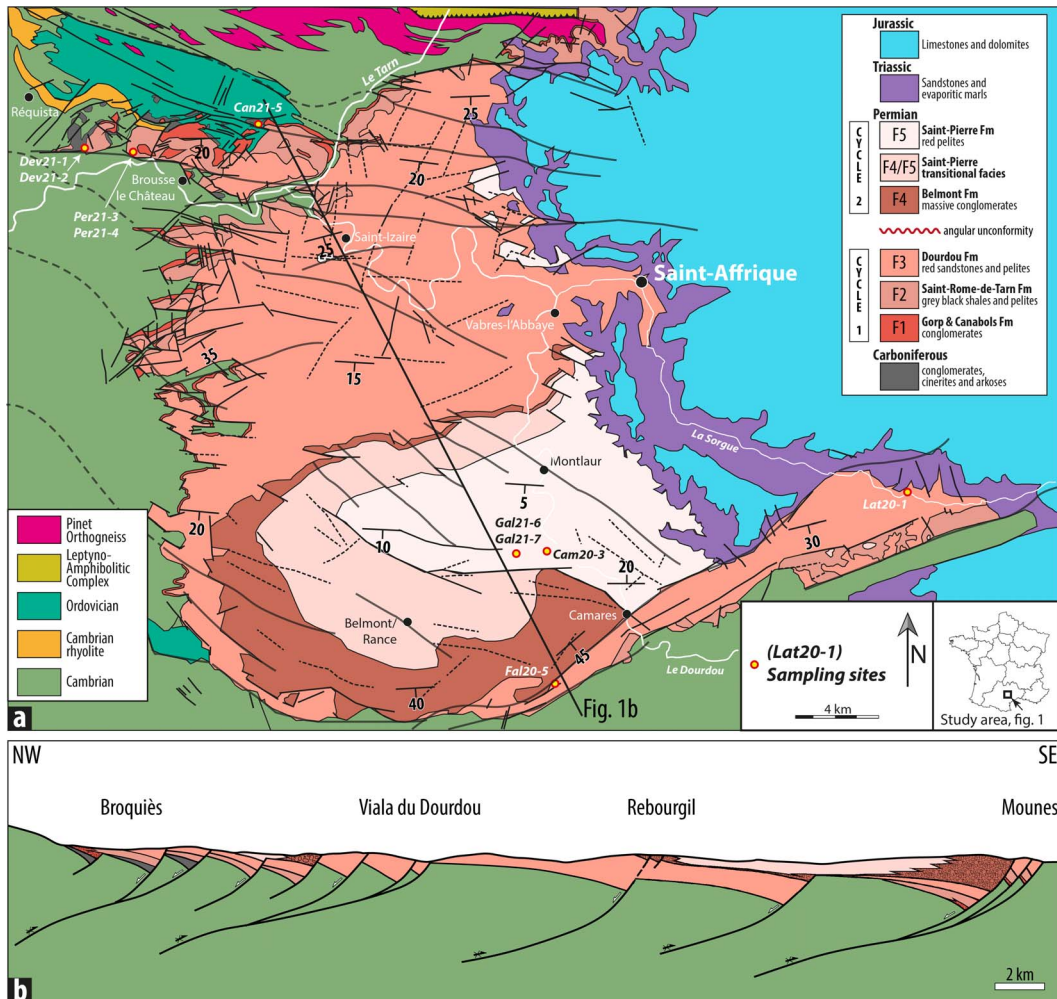


**Figure 1.** (A) Simplified geological map of the Saint-Affrique Basin [modified after Guérangé-Lozes and Guérangé, 1991, Guérangé-Lozes *et al.*, 1995 and Guérangé-Lozes and Alabouvette, 1999]; and (B) NWSE cross section of the Saint-Affrique Basin showing the successive back-faulting and southward migrating depocenter controlled by the rejuvenation and inversion of major Variscan thrusts [modified after Legrand, 1990].

the age and origin of these volcanic ash beds in order to shed light on the chronology of the Saint-Affrique Basin development and on the geodynamical setting prevailing south of the Massif Central at the end of the Variscan orogeny.

## 2. Geological setting

The Saint-Affrique Basin (Figure 1A) is one of the major intramountain Carboniferous–Permian continental basin from southwestern France [e.g. Rolando,

1988, Rolando *et al.*, 1988]. It is considered as an overall southward-dipping half-graben basin, controlled by repeated back faulting along major Variscan thrusts that were successively inverted during the late Carboniferous to Permian crustal thinning and collapse of the Variscan-related Montagne Noire thrust belt [Figure 1B; Legrand, 1990]. Most of the late Carboniferous to Permian deposits unconformably onlap onto the Precambrian to Cambro-Ordovician feldspathic sandstones and black schists of the Saint-Sernin-sur-Rance nappe, with a ma-

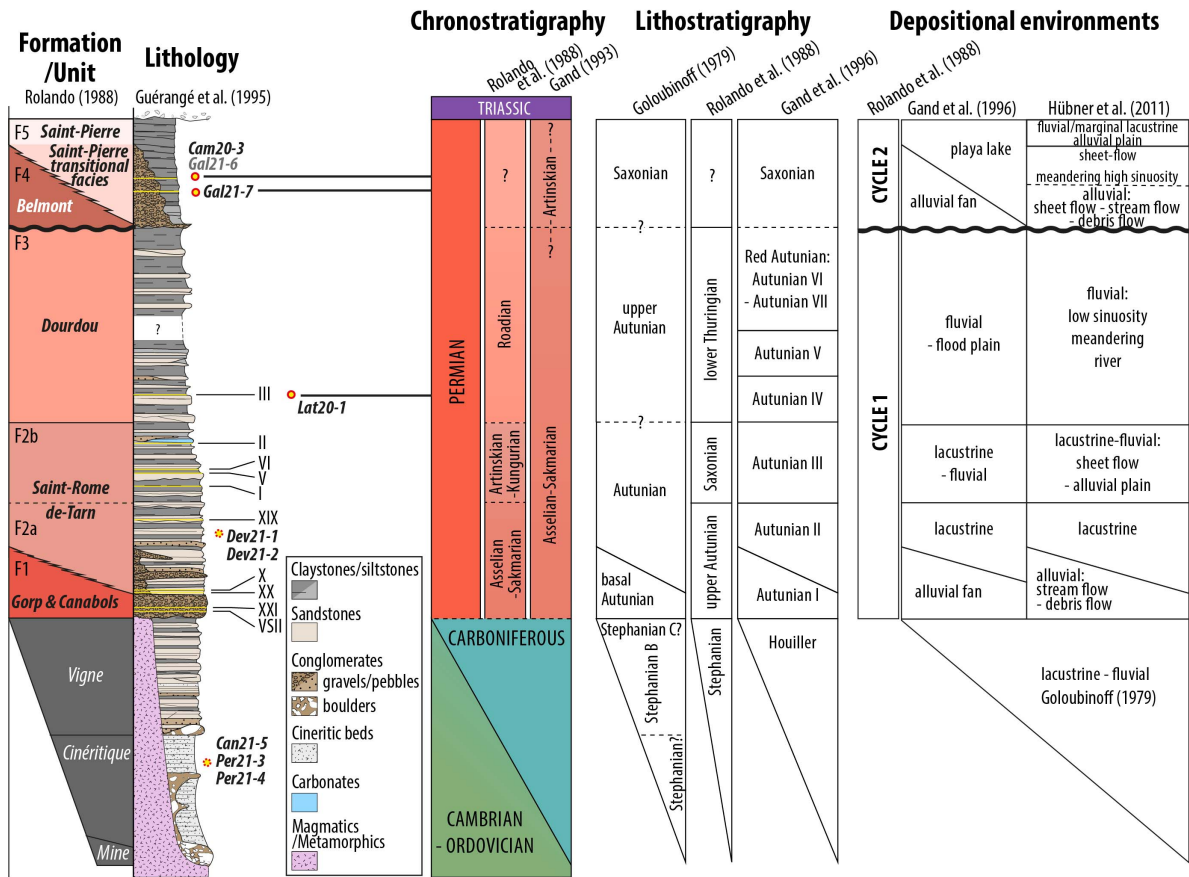


**Figure 2.** General description of the Saint-Affrique Basin sedimentary succession [based on Guérangé-Lozes et al., 1995] with the stratigraphic location of the selected volcanic ash bed samples, chronostratigraphic and lithostratigraphic subdivisions [after Goloubinoff, 1979, Rolando et al., 1988, Gand, 1993, Gand et al., 1996], and depositional environment evolution [after Goloubinoff, 1979, Rolando et al., 1988, Gand et al., 1996 and Hübner et al., 2011].

norward detrital input coming from the erosion of the uplifted northern limb of the Montagne Noire Massif. The latter includes Cambrian to Ordovician sandstone, shale and carbonate deposits of the metasedimentary cover, as well as gneisses, migmatites and biotite and garnet granites of the axial core complex. The tilted northern border of the basin is in turn fed by calc-alkaline metamonzogranites and metasyenogranites fringing the leptyno-amphibolite group of the Lézérou.

Syn-rift faulting controlled the asymmetric geometry, depositional partitioning and architecture of an overall alluvial to lacustrine sedimentation [Rolando, 1988, Legrand et al., 1994]. The stratigraphic range of the basin infill is assumed to cover the late

Carboniferous, with a low angular unconformity in the northern part of the basin, to the middle Permian [Figure 2; Rolando et al., 1988, Gand, 1993].

It has been reported that the late Carboniferous corresponds to the Stephanian continental subdivision and includes three main formations (fms): at the base, the *Mine* Formation (Fm) is composed of a coarse conglomerate and breccia package and is overlapped unconformably by volcanoclastic deposits, including fine-grained ash layers and volcanic breccias belonging to the *Cinérétique* Fm (Figure 2). The latter passes transitionally to the *Vigne* Fm, mainly composed of volcanic breccias alternating with coarse arkosic sandstones [David, 1967, Goloubinoff, 1979, Rolando, 1988; Figure 2].

The Permian deposits correspond to five formations accumulated during two sedimentary cycles. Cycle 1 corresponds to the F1, F2 and F3 fms and Cycle 2 to the F4 and F5 fms [Figure 2; Rolando *et al.*, 1988]. At the base, the F1 Fm, named the *Gorb and Canabols* Fm (Figure 1A and B), is mainly composed of stacked conglomerates considered as streamflow and debris flow deposits [Hübner *et al.*, 2011], passing laterally to fluvio-lacustrine deposits [Rolando, 1988]. The F2 Fm, named the *Saint-Rome-de-Tarn* Fm [Rolando, 1988], conformably overlays the F1 Fm and is divided into two lithologic units: the F2a Unit, described as lacustrine [Rolando, 1988, Hübner *et al.*, 2011], and the F2b Unit, considered as fluvio-lacustrine to lacustrine [Rolando, 1988], evolving upward into sheetflood to alluvial plain deposits [Hübner *et al.*, 2011]. This formation is overlain by the fluvial F3 Fm, named the *Dourdou* Fm [Rolando, 1988], interpreted as a low sinuosity meandering river system [Hübner *et al.*, 2011]. After a regional erosive event marked by a low angular unconformity, the F4 Fm, named the *Belmont* Fm, is attributed to the emplacement of alluvial-fan deposits during a major tectonic rejuvenation event from the southern border of the basin. The thick massive conglomerate package passes upwards and laterally to playa-lake deposits identified as the F5 Fm, named the *Saint-Pierre* Fm [Rolando, 1988; Figure 1A and B]. Hübner *et al.* [2011] consider that part of the F4 and F5 fms, denoted as F4/F5, i.e. the *Saint-Pierre transitional facies* Fm, is transitional and marks the lateral and vertical evolution from alluvial fan to meandering and alluvial plain deposits (Figure 2).

The stratigraphic setting of this sedimentary succession was firstly based on palynological analyses, i.e. defining continental floristic stages (Figure 2). Based on the microflora composition, i.e. spores and pollens, sediments of Cycle 1 were attributed to late Autunian to early Thuringian subdivisions [Rolando *et al.*, 1988]. However, using fauna biostratigraphy and in particular freshwater jellyfish, in comparison with German basins, Gand *et al.* [1996] proposed an early Asselian age for the F2b Unit, in which the species *Medusina atava* was identified, but they did not exclude that a simple paleoenvironment control could explain this fossil distribution in the stratigraphy. In turn, the upper part of the F3 Fm provided the *Medusina limnica* species which unfortunately

straddles a large stratigraphical repartition from the Sakmarian to the late Permian. By using climate-relevant geochemical, petrological and sedimentological proxies, Hübner *et al.* [2011] correlated the climate cycles from the Saint-Affrique and Lodève basins and proposed an Asselian to Artinskian age for Cycle 1 (F1, F2 and F3 fms), and an Artinskian age for the base of Cycle 2 (F4 and the base of F5 fms, Figure 2). As these stratigraphic interpretations based on fauna and flora depend on environmental and climate conditions, they lead to large age uncertainties thereby highlighting the need for absolute dating.

Several volcanic ash layers, named under the general term of cinerites, were described throughout the Carboniferous to Permian sedimentary succession [Goloubinoff, 1979, Rolando, 1988]. Some of these layers are reported as equivalent to those found in the Lodève Basin [Laversanne, 1976, Odin and Conrad, 1987]. Given their instantaneous deposition, these tuff beds are the best candidates to provide accurate absolute dating. In outcrops, they are easily identifiable by their pale-light colour (from white to salmon), their regular thickness and their hardness contrasting with the surrounding rocks. The major key tuff beds were identified in the *Cinéritique* Fm at the base of F1 Fm and in the F2 and F3 fms [Figure 2; e.g. Rolando, 1988]. In order to constrain the age of the sedimentary successions, six different volcanic ash and tuffitic beds have been collected throughout the stratigraphic column of the Saint-Affrique Basin (see Figure 1A).

### 3. Samples and methods

#### 3.1. Sampling

Eight samples have been collected in the entire basin (Figures 1A and 2 and Table 1). Three of them (Per21-3, Per21-4 and Can21-5) have been sampled in the so-called *Cinéritique* Fm belonging to the Stephanian subdivision, but due to lack of continuous outcrops, their precise stratigraphic location in this Fm is not known (Figures 1A and 2). One sample (Dev21-1) was collected in the *Saint-Rome-de-Tarn* Fm (F2), in the Grey Autunian subdivision (Figures 1A, B and 2). Another one (Lat20-1) is located within the *Dourdou* Fm (F3; Figures 1A, B, 2 and 3A) and corresponds to Rolando's cinerite III (1988). The remaining three samples (Gal21-6, Gal21-7 and Cam20-3) were collected within the *Saint-Pierre transitional facies* Fm

**Table 1.** GPS coordinates of the selected samples

| Samples | Locations  | Lat/long coordinates                |
|---------|--|-------------------------------------|
| Per21-4 | Along the road between the farm of Le Cluzel and the hamlet of Peret                         | 44° 0' 58.76" N<br>2° 34' 59.44" E  |
| Per21-3 | Near the hamlet of Peret   | 44° 1' 08" N<br>2° 35' 13" E        |
| Can21-5 | Along the road to the north-east of the Cansac hamlet  | 44° 1' 23" N<br>2° 40' 11" E        |
| Dev21-1 | Left bank of the Jauret creek  | 44° 00' 41" N<br>2° 35' 55" E       |
| Lat20-1 | Just outside the village of Latour-sur-Sorgues along the D7 road                             | 43° 47' 39" N<br>2° 50' 26" E       |
| Gal21-7 | Near the farm of Galamans along the road to the hamlet of Verrières, above the Riaudou creek | 43° 50' 50.36" N<br>2° 49' 12.88" E |
| Cam20-3 | Along the D999 road  | 43° 50' 47" N<br>2° 50' 5" E        |
| Gal21-6 | Same layer as sample Cam 20-3  | 43° 50' 47" N<br>2° 49' 02" E       |

(F4/F5), close to the top of the red Autunian subdivision (Figures 1A, B, 2 and 3B for sample Cam20-3).

### 3.2. Whole-rock geochemical analyses

Samples were crushed at Thin Section Lab (TSL, Toul, France) following a standard protocol to obtain adequate powder fractions using agate mortars. Chemical analyses (Supplementary Table 1) were performed by the Service d'Analyse des Roches et des Minéraux (SARM; CRPG-CNRS, Nancy, France) using an ICP-AES (inductively coupled plasma-atomic emission spectroscopy) for major-elements and an ICP-MS (inductively coupled plasma-mass spectrometry) for trace-elements, following the techniques described in Carignan *et al.* [2001]. All geochemical classification and tectonic discrimination diagrams used in this study were drawn using the GCDkit software [Janousek *et al.*, 2006].

### 3.3. Zircon U–Pb dating

A classic mineral separation procedure has been applied to concentrate zircon grains suitable for U–Pb dating using the facilities available at TSL. Zircon grains were imaged by cathode luminescence (CL)

using a Reliotron CL system equipped with a digital colour camera available at the GeOHeLiS platform (University of Rennes 1, France).

U–Pb geochronology of zircon was conducted by in-situ LA–ICP–MS (laser ablation–inductively coupled plasma–mass spectrometry) at the GeOHeLiS analytical platform using an ESI NWR193UC Excimer laser (193 nm wavelength), coupled to a quadrupole Agilent 7700x ICP–MS equipped with a dual pumping system to enhance sensitivity [Paquette *et al.*, 2014]. The methodology used to perform the analyses can be found in Nosenzo *et al.* [2022] as well as in Supplementary Table 2. Concordia diagrams have been generated using IsoplotR [Vermeesch, 2018].

### 3.4. Zircon Hf analyses

Lu–Hf isotopes were measured at the Géosciences Montpellier Laboratory, University of Montpellier (AETE–ISO regional facility of the OSU OREME) using a ThermoFinnigan Neptune+ MC–ICP–MS (multicollector–inductively coupled plasma–mass spectrometer) coupled with a Photon-Machine Analyte G2 Excimer laser (193 nm wavelength). Ablation was performed using a 50 µm spot size. The laser frequency was 5 Hz and the energy density of the

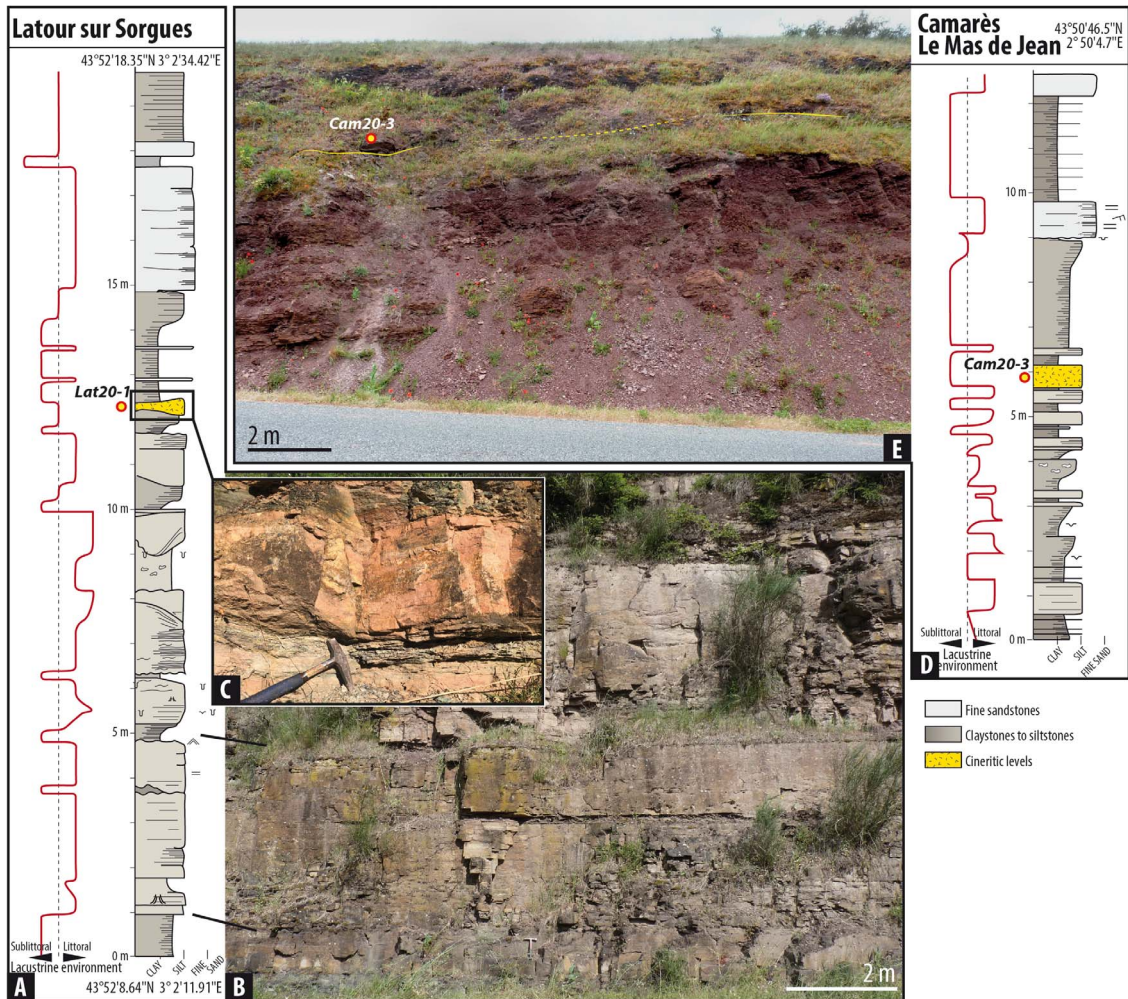


**Figure 3.** (A) Detailed sedimentary section of the outcrop of Latour-sur-Sorgues located along the D7 road, where sample Lat20-1 was collected; (B) Photography of the base of the section; (C) Photography of the cineritic bed providing the Lat20-1 sample; (D) Detailed sedimentary section of the outcrop of Le Mas de Jean located near the Camarès village along the D999 road, where sample Cam20-3 was collected; (E) Photography of the outcrop with the stratigraphic location of the cinerite providing the Cam20-3 sample.

laser beam was  $c. 6 \text{ J/cm}^2$ . A typical analysis was 80 s, including a 40 s background measurement and a 40 s ablation period. The correction for the interferences and mass bias followed the procedure outlined in previous reports [e.g. Bruguier *et al.*, 2020]. The correction for the isobaric interference of Yb and Lu on  $^{176}\text{Hf}$  was made following a method detailed in Fisher *et al.* [2011]. For Yb, the interference-free  $^{171}\text{Yb}$  was corrected for mass bias effects using an exponential

law and  $^{173}\text{Yb}/^{171}\text{Yb} = 1.130172$  [Segal *et al.*, 2003]. The mass bias-corrected  $^{171}\text{Yb}$  was monitored during the run and the magnitude of the  $^{176}\text{Yb}$  interference on  $^{176}\text{Hf}$  was calculated using  $^{176}\text{Yb}/^{171}\text{Yb} = 0.897145$  [Segal *et al.*, 2003]. For Lu, the interference-free  $^{175}\text{Lu}$  was corrected for mass bias effects assuming  $\beta\text{Lu} = \beta\text{Yb}$  and using an exponential law. The mass bias-corrected  $^{175}\text{Lu}$  was monitored during the run and the magnitude of the  $^{176}\text{Lu}$  interference on  $^{176}\text{Hf}$



was calculated using  $^{176}\text{Lu}/^{175}\text{Lu} = 0.02655$  [Vervoort *et al.*, 2004]. Interference-corrected  $^{176}\text{Hf}/^{177}\text{Hf}$  were corrected for mass bias using an exponential law and  $^{179}\text{Hf}/^{177}\text{Hf} = 0.7325$  [Patchett *et al.*, 1981]. Initial Hf isotope ratios and  $\epsilon\text{Hf}$  values were calculated using the decay constant for  $^{176}\text{Lu}$  of  $1.867 \times 10^{-11} \text{ yr}^{-1}$  [Söderlund *et al.*, 2004] and the CHUR values of 0.282785 and 0.0336 for  $^{176}\text{Hf}/^{177}\text{Hf}$  and  $^{176}\text{Lu}/^{177}\text{Hf}$  [Bouvier *et al.*, 2008]. The accuracy and long-term reproducibility of the measurements were gauged by analysing three zircon reference standards [91,500, GJ1 and Plešovice with reference values taken from Blichert-Toft, 2008, Morel *et al.*, 2008, Sláma *et al.*, 2008, respectively] and all values were found to be in agreement with the reference values: 91,500 ( $^{176}\text{Hf}/^{177}\text{Hf} = 0.282298 \pm 24$ ,  $n = 30$ ), Plešovice ( $^{176}\text{Hf}/^{177}\text{Hf} = 0.282473 \pm 19$ ,  $n = 13$ ) and GJ1 ( $^{176}\text{Hf}/^{177}\text{Hf} = 0.282007 \pm 32$ ,  $n = 15$ ) (all errors at 2 s.d. level).

## 4. Results

### 4.1. Petrology

Sample Per21-4, from the *Cinéritique* Fm (Figures 1A and 2), is a tuffite characterized by a centimetric-scale layering related to grain size alternation. In thin section, it is dominated by a very fine-grained matrix including floating flat parallel unsorted silt to rare coarse sand-size clasts responsible for the laminated fabric. The clast fraction is mainly composed of large elongated quartz grains including micro bubble-like cavities compatible with ancient glass shards, K-feldspars and abundant muscovite flakes (Figure 4A). Secondary carbonates can also be observed.

Also from the *Cinéritique* Fm (Figure 2), the matrix of sample Can21-5 was collected in a 20 cm thick light-beige layer containing numerous plant remnants. It is extremely fine-grained and contains a dispersed very-fine silt-size fraction, including resorbed quartz crystal clasts (Figure 4B) and K-feldspar clasts, consistent with a pyroclastic origin, as well as terrigenous muscovite flakes.

Sample Dev21-1 corresponds to a 5 cm thick very fine-grained light-grey layer belonging to the *Saint-Rome-de-Tarn* Fm (Figures 1A and 2). In thin section (Figure 4C), it is composed of an extremely fine-grained matrix-supported silt- to sand-size unsorted clastic fraction, including larger angular to subangular quartz fragments of possible altered glass shards,

K-feldspar clasts, as well as rare tiny terrigenous muscovite flakes, indicating the lack of hydrodynamical sorting (Figure 4C).

Sample Lat20-1 belongs to the *Dourdou* Fm (F3 Unit, Figures 1A, 2 and 3A). It is a pinkish to light-beige fine-grained tuff with an eutaxitic-like fabric marked by black flame-like structures, suggesting a pyroclastic flow deposit, rather than a fall deposit. In thin section (Figure 4D), the sample is highly recrystallized and displays an anhedral quartz-rich mosaic invading the residual cryptocrystalline matrix with large dispersed carbonate patches and remaining K-feldspar and plagioclase clasts. A striking feature is the strong late carbonatation and recrystallization that this tuff suffered, possibly during the diagenetic processes.

Sample Gal21-7 belongs to the *Saint-Pierre* Fm (F5 Fm, Figure 2). In thin section, it is characterized by a dominant cryptocrystalline matrix, probably at least partly vitreous, containing millimetre thick bands enriched with fine sand-size to silt-size quartz and K-feldspar debris, together with smaller biotite and detrital muscovite grains. As shown on Figure 4E, some of the quartz clasts show resorption gulfs, which is consistent with their interpretation as rhyolitic quartz that underwent fast decompression in volcanic conduits. Lithic fragments, among which angular polycrystalline quartz clasts, can also be found.

Samples Cam20-3 and Gal21-6 were sampled in the same 20 cm thick tuffitic layer of the *Saint-Pierre* Fm (F5, Figures 1A, 2 and 3B). Sample Cam20-3 is a light-grey tuffite with a centimetric scale layering. In thin section, it contains a fair number of lithic fragments and angular quartz clasts (Figure 4F) compatible with a pyroclastic origin, as well as K-feldspar and plagioclase clasts together with chlorite after biotite, muscovite, accessory tourmaline and opaque minerals into a cryptocrystalline matrix. Muscovite and tourmaline indicate a mixing of the pyroclastic content with a terrigenous input. As shown on Figure 4F, this sample also reveals the presence of secondary carbonate minerals. Sample Gal21-6 is a very fine-grained tuffite similar to sample Gal21-7, but with a much smaller grain size with a clear planar microfabric marked by the alignment of the quartz clasts and muscovite microdebris (Figure 4G). Some late goethite veins can be found in this sample (Figure 4G).

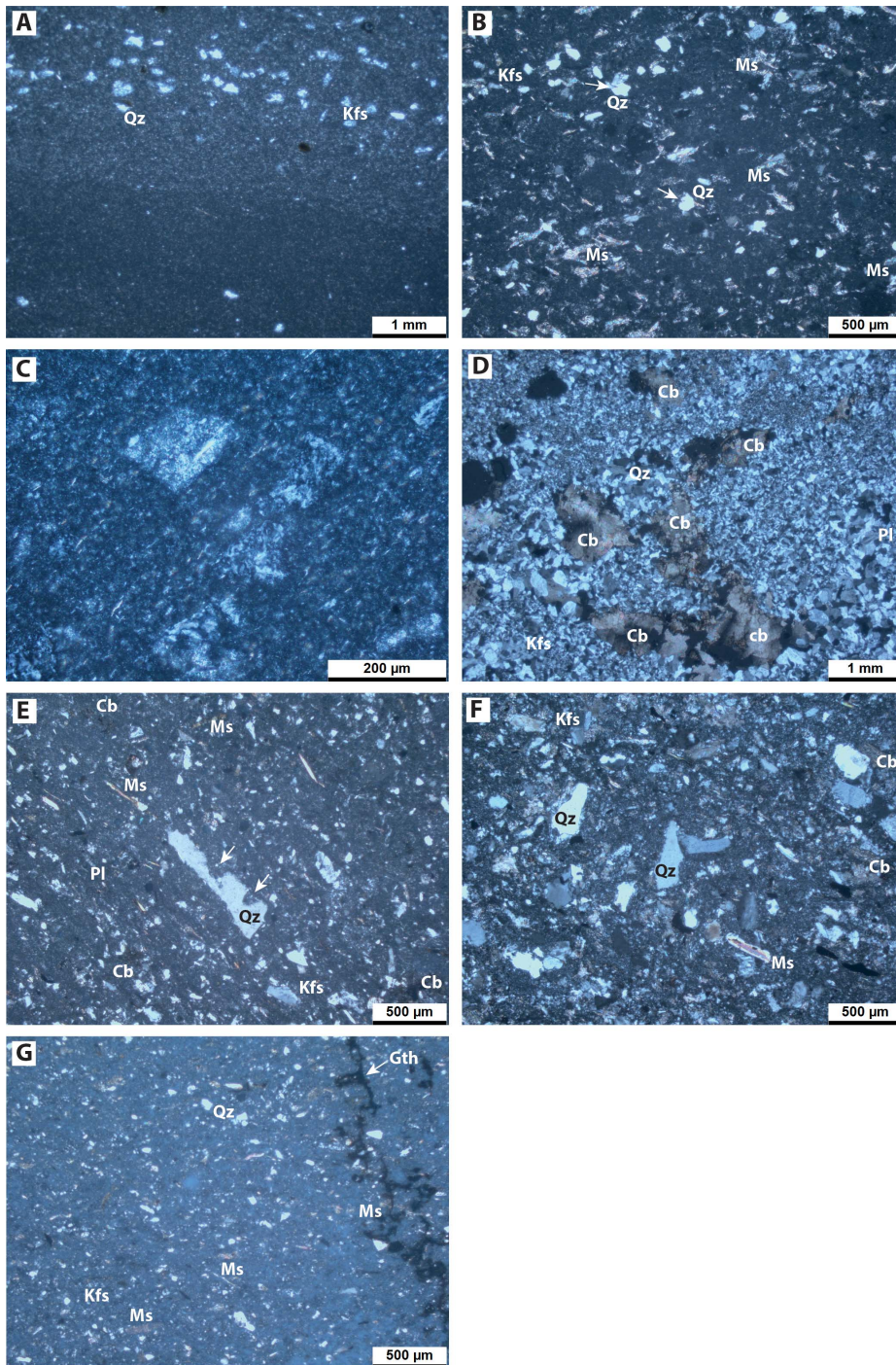


**Figure 4.** Optical cross-polarized light microphotographs for the samples from the Saint-Affrique Basin. (A) Sample Per21-4; note the layering marked by the variations of granulometry. (B) Sample Can21-5; white arrows show resorbed quartz grains. (C) Sample Dev21-1. (D) Sample Lat20-1; note the strong carbonatation. (E) Sample Gal21-7; white arrows show a decompression-related resorbed quartz crystal. (F) Sample Cam20-3; note the presence of angular quartz fragments. (G) Sample Gal21-6; note the presence of late goethite veins. Mineral abbreviations: Cb carbonate minerals; Gth goethite; Kfs K-feldspar; Ms muscovite; Pl plagioclase; Qz; quartz.

#### 4.2. Whole-Rock geochemistry

Eight samples have been selected for major and trace element analyses (Supplementary Table 1). As illustrated in the previous section, all samples consist of ash tuffs and tuffites in which the terrigenous input is variable but obviously difficult to accurately quantify for each of the samples, a feature that may disturb their volcanic geochemical signatures. In addition, some samples underwent late (i.e. post-deposition) diagenetic modifications, such as carbonatation, sometimes fairly important, as for sample Lat20-1 that contains more than 10 wt% CaO. This increase in CaO (and Sr) content consequently dilutes the other elements. These characteristics can limit the usefulness of geochemical diagrams, which therefore need to be used with caution, especially those based on major element concentrations. In the conventional total alkali-silica (TAS) diagram (Figure 5A), sample Lat20-1 plots in the field of basaltic trachy-andesite, while all the others plot in the rhyolite field.

Whole-rock immobile trace and REE elements are often used in the case of volcanic ashes studies as they are usually less sensitive to post deposition processes (such as diagenesis). In the Zr/TiO<sub>2</sub> versus Nb/Y diagram of Winchester and Floyd [1977], two distinct groups appear (Figure 5B). A first group, comprising Per21-4, Per21-3, Can21-5 and Dev21-1 plots in the field of trachyte/trachy-andesite whereas a second group (Gal21-6, Gal21-7, Cam20-3 and Lat20-1) plots in the rhyodacite/dacite field. It should be noticed that yttrium can be lost during the alteration of volcanic rocks [Hill *et al.*, 2000] and therefore the alkalinity attributed to the samples should be considered as a maximum estimate.

In a Primitive Mantle normalized multi-elements diagram [McDonough and Sun, 1995, Figure 6a], all the studied samples yield trends that are comparable with the Upper Continental Crust [UCC, Taylor and McLennan, 1985]. Overall, the samples show a strong enrichment in LREE (Figure 5B), and, with the exception of sample Dev21-1, a negative Eu/Eu\* anomaly, often found in felsic volcanic rocks [Wray, 1999]. In further detail, it is noteworthy that samples belonging to the two groups defined above present two distinct trends overall (Supplementary Table 1 and Figure 6B). Samples from the first group (Per21-4, Per21-3, Can21-5 and Dev21-1) display a low REE content

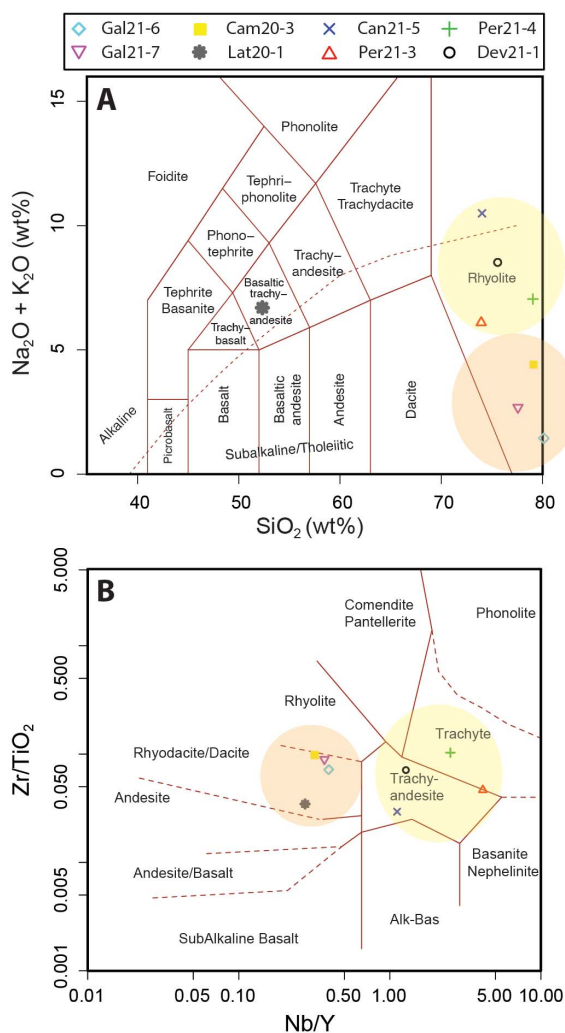


**Figure 5.** Geochemical classification diagrams for the samples collected within the Saint-Affrique Basin. (A) Total alkali-silica diagram [TAS, Le Maitre *et al.*, 1989]; (B) Zr/TiO<sub>2</sub> versus Nb/Y diagram [Winchester and Floyd, 1977]. The yellow ellipse corresponds to the first group of samples; the orange one to the second group of samples.

(22 to 98 ppm), a less pronounced negative Eu/Eu\* anomaly (0.65 to 0.98) and strong HREE depletions. In contrast, samples from the second group (Gal21-6, Gal21-7, Cam20-3 and Lat20-1) present a higher REE content (143 to 158 ppm), a more pronounced Eu/Eu\* anomaly (between 0.17 to 0.69) and flat HREE patterns. If the REE contents are normalized to that

of the Cody shale [Figure 6C; Jarvis and Jarvis, 1985], most samples show a negative Eu anomaly, are depleted in LREE and are either flat (second group) or depleted (first group) in HREE, which are all typical features for volcanic ashes [Wray and Wood, 1998, Ducassou *et al.*, 2019]. The fact that trend for Dev21-1 is fairly flat (Figure 6C) is often characteristic of a non-negligible detrital input [Wray and Wood, 1998, Ducassou *et al.*, 2019].

In the tectonic discrimination diagram (Figure 7A) presented by Schandl and Gorton [2002], the first group of previously defined (see above) samples plots in the “Within Plate Volcanic Zones” field while the second group plots in the “Active Continental Margin” field. In the tectonic diagram of Wood [1980], based on Hf/3–Th–Ta (Figure 7B), the second group of samples is characterized by a calc-alkaline chemistry, while the first group displays a higher Ta content relative to Th and Hf.

### 4.3. U–Pb dating of zircon

Unfortunately, it was not possible to find any minerals suitable for U–Pb dating in samples Per21-3 and Dev21-1.

Very few zircon grains were present in sample Per21-4 (*Cinéritique* Fm). Nine grains with various sizes were analyzed (Supplementary Table 3). They yielded variable U and Pb contents and fairly consistent Th/U ratios. With the exception of three discordant analyses (Figure 8A), three age groups can be defined: a first one around 2.0 Ga, a second one around 1.0 Ga and the last one around 0.6 Ga.

Again, very few zircon grains were found in sample Can21-5 (*Cinéritique* Fm). Thirteen grains with variable sizes were analyzed. They yield very high U (up to 3220 ppm) and Pb (up to 7648 ppm) contents (Supplementary Table 3) together with very high common Pb contents (f206c up to 39%). Their Th/U ratios are also highly variable (from 0.03 up to 0.53). Reported in a Concordia diagram (Figure 8B) they plot mostly in a discordant position with the exception of two grains (Zr12 and 13) which are concordant around 2.0 Ga.

Twenty-four analyses out of sixteen different zircon grains were acquired for sample Lat20-1 (Figure 3A; Supplementary Table 3). All zircon grains were prismatic, ranging in size between 70 and 200  $\mu\text{m}$  and with simple concentric zoning (Figure 9).

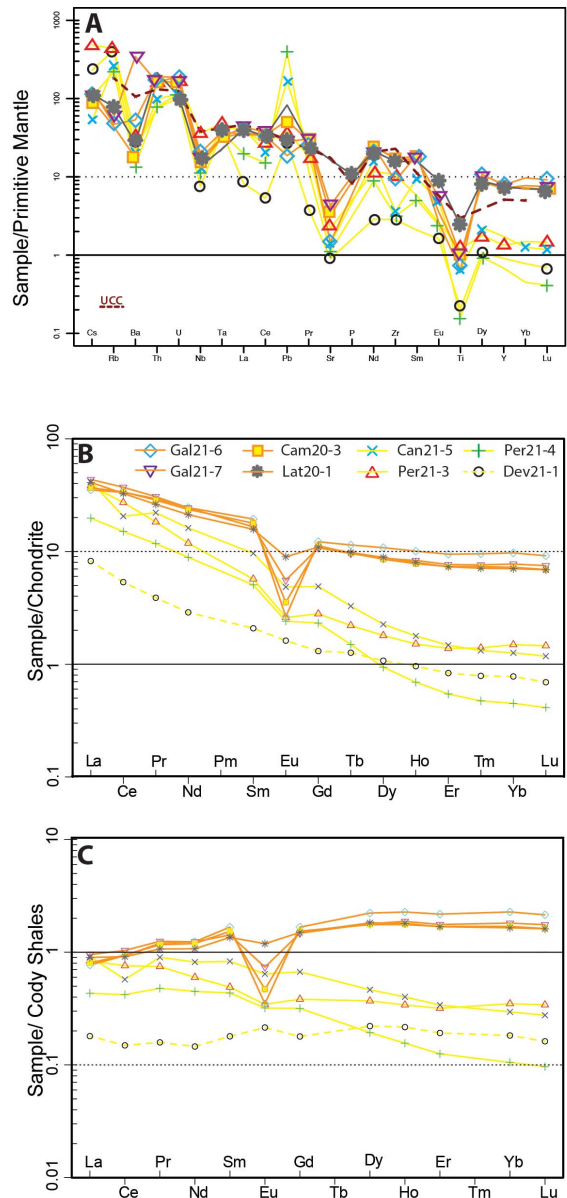


**Figure 6.** (A) Multi-element diagram normalized to Primitive Mantle [Sun and McDonough, 1989]. UCC = upper continental crust [Taylor and McLennan, 1985]; (B,C) Rare earth element plots for the tuff samples collected within the Saint-Affrique Basin. REE data are normalized (B) to the CI-chondrite [McDonough and Sun, 1995] and (C) to the Cody Shale [Jarvis and Jarvis, 1985]. Yellow lines correspond to the first group of samples; the orange line to the second group of samples.

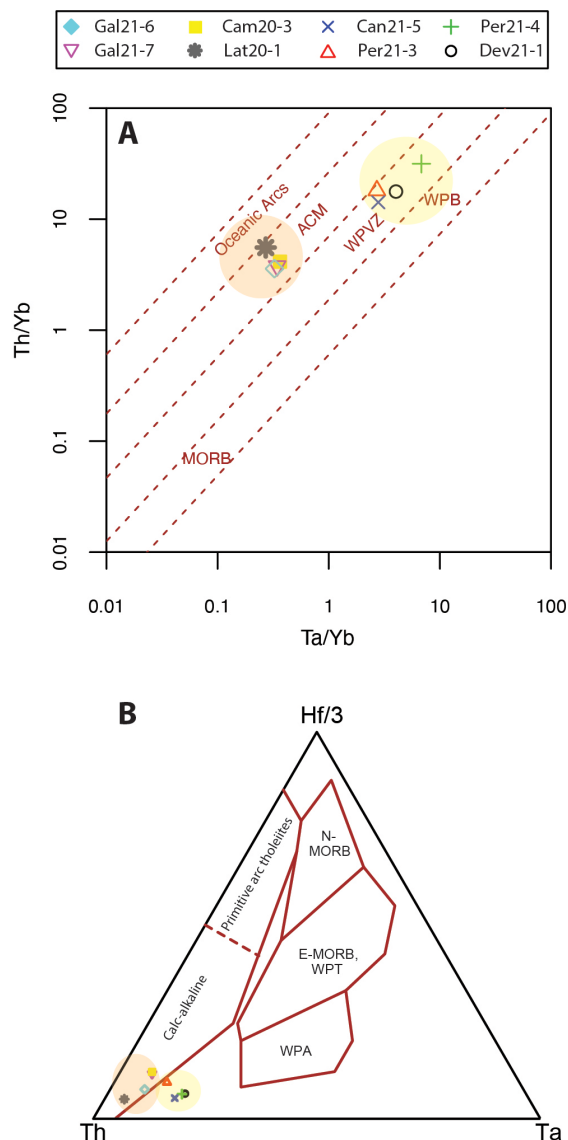


**Figure 7.** (A) Th/Yb versus Ta/Yb tectonic discrimination diagrams [after Schandl and Gorton, 2002]. ACM = active continental margin, MORB = mid-ocean ridge basalts, WPB = within plate basalts, WPVZ = within plate volcanic zones; (B) Hf/3–Th–Ta triangular diagram [after Wood, 1980]. WPA = within plate alkaline basalts and differentiates, WPT = within plate tholeiitic basalts and differentiates. The yellow ellipse corresponds to the first group of samples; the orange one to the second group of samples.

They yield variable U (236 to 9651 ppm) and Pb (50 to 908 ppm) contents with Th/U ratios consistent with a magmatic origin [0.1 to 0.26; see Witt *et al.*, 2017 and references therein]. Eighteen analyses plot in a concordant position (Figure 8C) and yield a concordia date of  $280.3 \pm 2.6$  Ma (MSWD = 1.2). Two analyses (Zr 1.1 and Zr 11.2, Supplementary Figure 1) were acquired on grains that contain a non-negligible common Pb content (f206c of 1.56 and 6.38% respectively) and that probably belong to the same age group. Two analyses acquired on the same grain (Zr2) plot in a concordant position with apparent  $^{206}\text{Pb}/^{238}\text{U}$  ages of around 320 Ma (Supplementary Figure 1), whereas a last analysis (Zr12, containing a non-negligible amount of common Pb; f206c% = 6.4), is highly discordant (52%; Supplementary Figure 1).

Thirty-one analyses (Supplementary Table 3) out of thirty-one different zircon crystals were acquired for sample Gal21-7 (Figures 1A and 2). Most crystals are rather elongated (up to 250  $\mu\text{m}$ ) and most of them display simple concentric magmatic zoning (Figure 9). Here again, the U (108 to 1886 ppm) and Pb (35 to 875 ppm) contents are highly variable. All the Th/U ratios, however, are compatible with a magmatic origin (0.13 to 0.48). A group of twenty-nine analyses (Figure 8D) define a concordia date of  $278.4 \pm 2.3$  Ma (MSWD = 1.6). One grain (Zr5), characterized by a non-negligible common Pb content (f206c = 1.1%), plots to the right of the main batch of analyses and probably belongs to the same age group. The last analysis (Zr15) yields a concordant date around 470 Ma.

Thirty-two analyses (Supplementary Table 3) were acquired out of thirty-one zircon grains for sample Cam20-3 (Figure 3B). Zircon grains are generally prismatic with sizes ranging from 50 to 200  $\mu\text{m}$  and display a magmatic zoning when imaged by cathode luminescence (Figure 9). They present variable U (212 to 1757 ppm) and Pb (41 to 1162 ppm) contents, with Th/U ratios ranging from “typical” metamorphic (0.03 to 0.09) to magmatic (0.16 to 0.62). Four age groups can be identified (Figure 8E and Supplementary Figure 1). The oldest zircon (Zr 27) yields an apparent  $^{207}\text{Pb}/^{206}\text{Pb}$  age of ca. 2646 Ma (Supplementary Figure 1). One grain (Zr 25) yields a concordant date of ca. 940 Ma (Supplementary Figure 1). A third group of six zircon grains (Zr 1, 7, 8, 11, 17 and 20) returns apparent ages around 450–460 Ma

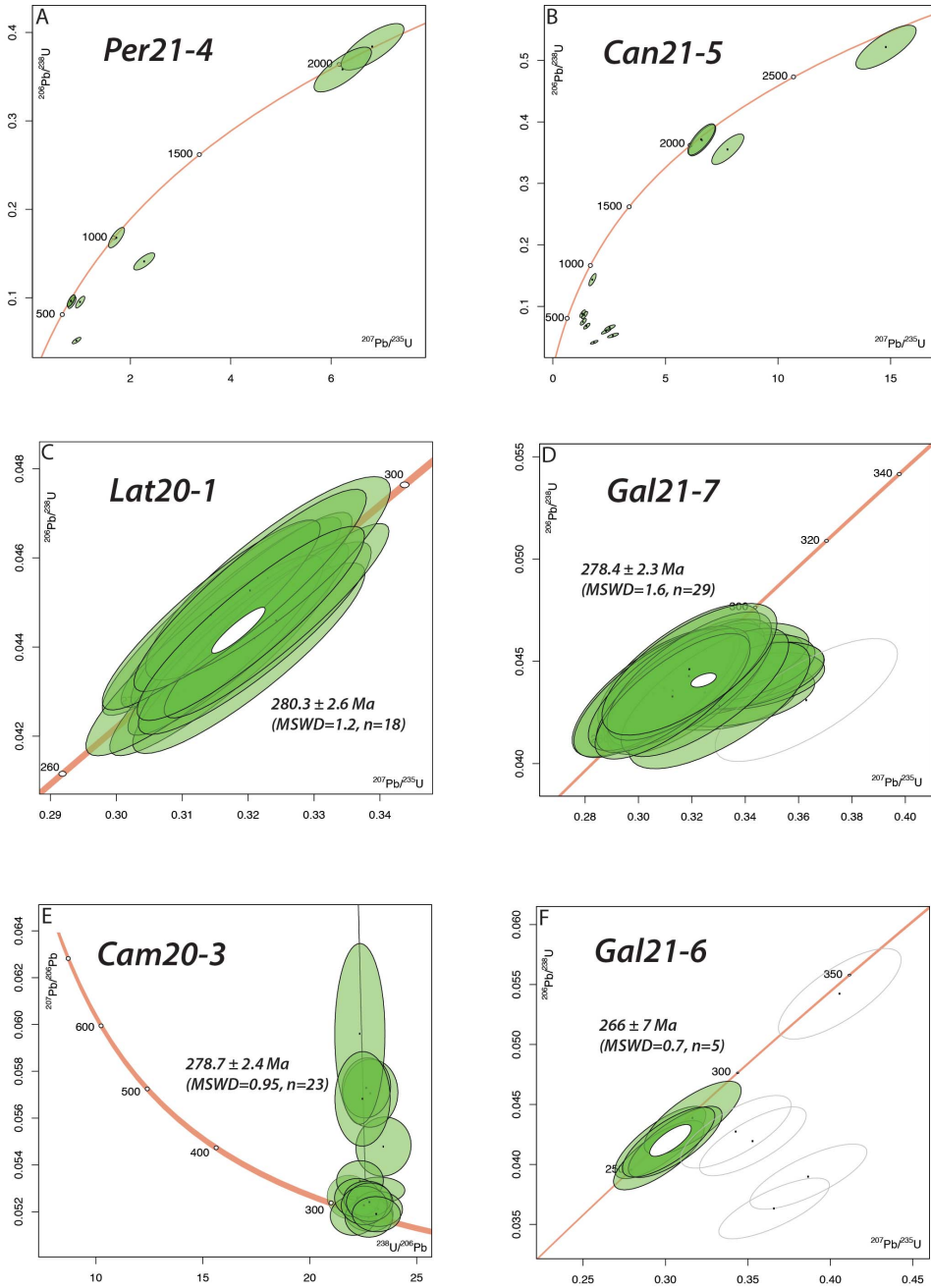


**Figure 8.** (A) Wetherill concordia diagram for sample Per21-4; (B) Wetherill concordia diagram for sample Can21-5; (C) Wetherill concordia diagram for sample Lat20-1; (D) Wetherill concordia diagram for sample Gal21-7; (E) Tera-Wasserburg concordia diagram for sample Cam20-3; (F) Wetherill concordia diagram for sample Gal21-6. MSWD = Mean Square Weighted Deviation.  $n$  = number of analyses used to calculate the U–Pb dates. All MSWD are calculated for concordance + equivalence. Grey ellipses were not used for age calculation.

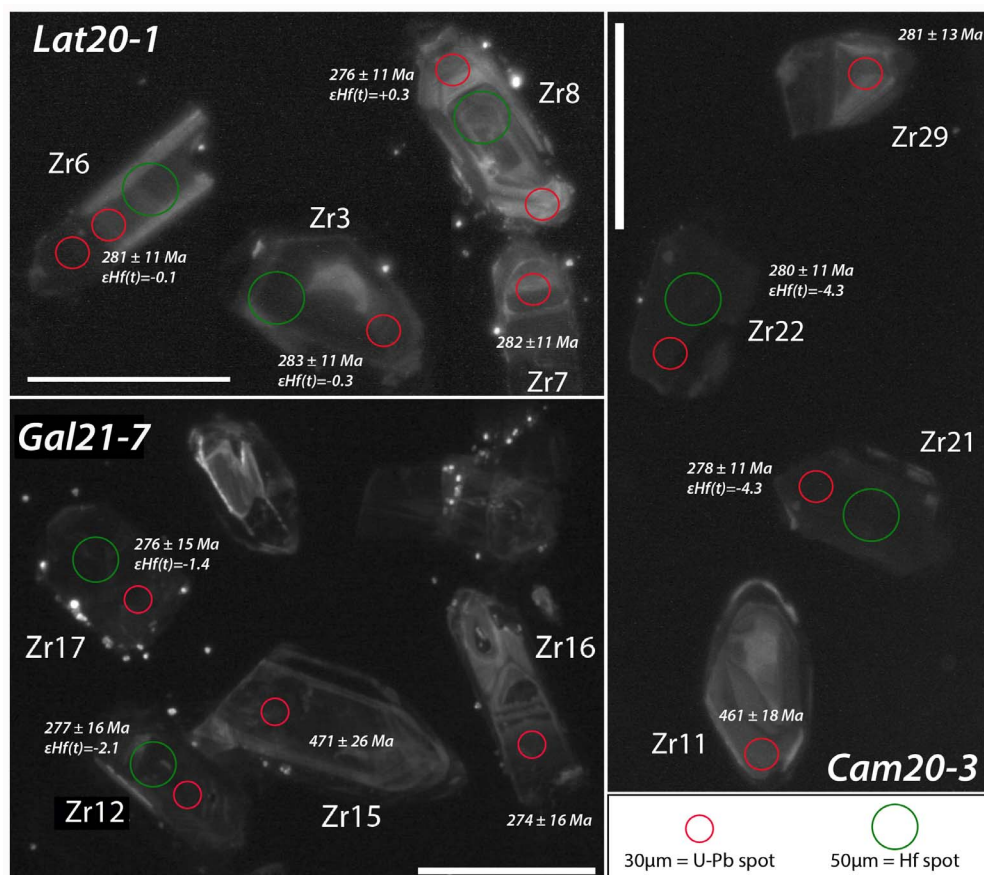


**Figure 9.** Cathode-luminescence imaging of some of the analyzed zircon grains. The white bar represents 200  $\mu\text{m}$ .

(Supplementary Figure 1), yielding the lowest (metamorphic?) Th/U ratios. The youngest group composed of twenty-three different zircon grains (Figure 8E) yields a lower intercept date of  $278.7 \pm 2.4 \text{ Ma}$  (MSWD = 0.95).

Ten zircon grains were found in sample Gal21-6 (Figure 1A and 2; Supplementary Table 3). All the grains were prismatic with concentric magmatic zoning (not shown). They are rich in U (up to 2558 ppm) and Pb (up to 1393 ppm), with fairly consistent Th/U ratios characteristic of magmatic sources (0.21 to 0.66). With the exception of one grain (Zr1) with a concordant date around 340 Ma (Figure 8F), the remaining five concordant analyses yield a concordia date of  $266 \pm 7 \text{ Ma}$  (MSWD = 0.7,  $n = 5$ ), whereas the oldest concordant zircon from this group has a  $^{206}\text{Pb}/^{238}\text{U}$  apparent age of  $277 \pm 15 \text{ Ma}$ . The four

other analyses are discordant with variable amount of common Pb ( $f_{206\text{c}}$  up to 2.78%).

#### 4.4. Zircon Hf isotope composition

Three samples were selected for zircon Hf isotope measurements (Lat20-1, Cam20-3 and Gal21-7, Supplementary Table 3).

For each sample, ten zircon grains (eleven for sample Cam20-3), previously analysed for U–Pb, were targeted for Hf isotopes. Hf analyses were done as close as possible to the U–Pb ablation pits. The results are reported in Figure 10.

For sample Lat20-1, the analyzed zircon grains display very low  $^{176}\text{Lu}/^{177}\text{Hf}$  ( $0.0009 \pm 1$ ) and initial (calculated at 280 Ma)  $^{176}\text{Hf}/^{177}\text{Hf}$  ranging from 0.282600 to 0.282630, with nearly chondritic  $\epsilon_{\text{Hf}}(t)$

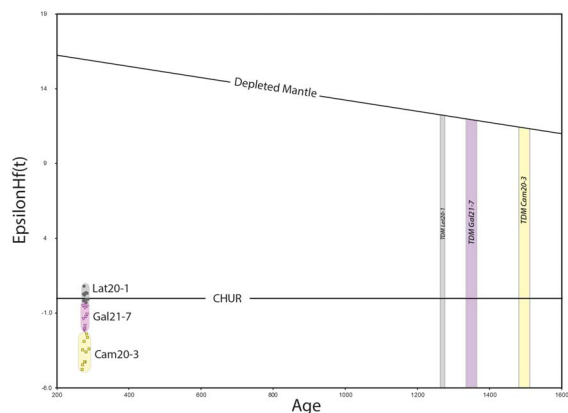


**Figure 10.**  $\epsilon\text{Hf}(t)$  versus  $^{206}\text{Pb}/^{238}\text{U}$  age of some selected zircon grains from samples Lat201, Gal21-7 and Cam20-3. Depleted Mantle and New Crust evolutions after Dhuime *et al.* [2011].

values (Figure 10) ranging from 0.8 to  $-0.3$  (mean  $0.1 \pm 0.2$ ).  $T_{\text{DM}}$  model ages are broadly similar to those measured from the two other samples and display a mean value of  $1269 \pm 13$  Ma.

Zircons from sample Gal21-7 (Supplementary Table 3) yield low  $^{176}\text{Lu}/^{177}\text{Hf}$  ( $0.0019 \pm 3$ ) and a mean  $^{176}\text{Hf}/^{177}\text{Hf}_i$  of  $0.282576 \pm 12$  (calculated at 278 Ma).  $\epsilon\text{Hf}(t)$  are slightly sub-chondritic (Figure 10), ranging from  $-0.3$  to  $-2.1$  (mean =  $-1.2 \pm 0.4$ ). The  $T_{\text{DM}}$  mean value is  $1352 \pm 27$  Ma.

For sample Cam20-3, the analyzed zircon grains present low  $^{176}\text{Lu}/^{177}\text{Hf}$  ratios ( $0.0024 \pm 6$ ) and homogeneous  $^{176}\text{Hf}/^{177}\text{Hf}_i$  ratios ( $0.282507 \pm 15$ ) calculated at 279 Ma. The corresponding initial  $\epsilon\text{Hf}$  are subchondritic, with values ranging from  $-4.8$  to  $-2.4$ , and a mean  $\epsilon\text{Hf}(t)$  of  $-3.6 \pm 0.5$  (Figure 10). Their  $T_{\text{DM}}$  yield a mean value of  $1507 \pm 33$  Ma. One xenocryst, dated at 454 Ma, was also analyzed and provides a distinct, slightly supra-chondritic  $\epsilon\text{Hf}(t)$  of 1.0.

## 5. Discussion

### 5.1. Age and nature of the volcanism in the Saint-Affrique Basin

Two groups of samples can be distinguished among the studied samples.

The first group of volcanoclastic beds (Can21-5, Per21-3, Per21-4 and Dev21-1) belonging to the

*Cin ritique* Fm (Figures 1A and 2), with a proposed Stephanian age (i.e. late Carboniferous), contains clasts (quartz and K-feldspars) that are consistent with a volcanic origin, and a fairly large detrital component. In the  $\text{Zr}/\text{TiO}_2$  versus  $\text{Nb}/\text{Y}$  diagram (Figure 5B, yellow ellipse) they plot in the field of trachyte/trachy-andesite, and they yield trace-element contents compatible with a felsic composition. They all have a calc-alkaline chemistry and exhibit “Within Plate Volcanic Zone”-like characteristics in the volcano-tectonic diagram of Wood [1980]; these features are compatible with a late to post-collisional volcanism. Sample Dev21-1, belonging to the *Saint-Rome-de-Tarn* Fm (i.e. proposed lower Cisuralian in age), exhibits a flat REE pattern when normalized to shale (Figure 6C), but also displays a “Within Plate Volcanic Zone” geochemical composition (Figure 7B). Unfortunately, it was not possible to date these samples because of the absence of volcanic zircon grains. The detrital zircon grains found in two of these samples demonstrates however the existence of a complex basement underneath and/or aside the Saint-Affrique Basin with ages ranging from the Paleo- to the Neo-Proterozoic (Figure 8A and B).

The second group of samples belong either to the *Dourdou* Fm (Lat20-1) or to the *Saint-Pierre* Fm (Gal21-6 and 21-7 and Cam20-3). These formations were so far attributed to the Sakmarian and Artinskian, respectively [Gand, 1993]. Although these samples have a fair amount of muscovite indicating a terrigenous contribution, and can be sometime affected by a strong carbonation (Lat20-1), they all contain clasts of feldspars and quartz demonstrating the presence of a rather important volcanic content. These samples can be classified as dacites/rhyodacites, have a strong negative  $\text{Eu}/\text{Eu}^*$  anomaly, a significant LREE enrichment and a fairly flat HREE spectrum; these features are all in a good agreement with their felsic nature, and can be defined as calc-alkaline rocks. All of these features are in a good agreement with a post-orogenic deposition setting. All of these samples provided volcanic zircon grains. The stratigraphically oldest sample from this group (Lat20-1) records a volcanic episode during the Kungurian. The obtained date of  $280 \pm 2.6$  Ma for this sample is interpreted as the age of the deposition of the bed, assuming that the dated zircon grains were not reworked after the volcanic eruption [e.g. Rossignol *et al.*, 2019]. Applying the same assump-



tion, the samples at the top of the sedimentary succession were then deposited at  $278.4 \pm 2.3$  Ma (Gal21-7) and  $278.7 \pm 2.4$  Ma (Cam20-3) respectively, i.e. also during the Kungurian. The date of  $266 \pm 7$  Ma found for sample Gal21-6 may be related to slight Pb losses enhanced by the zircon's high U content ( $>1500$  ppm) and has to be considered as a minimum age of deposition, as this sample belongs to the same ash bed as Cam20-3. Therefore, we propose that the date of  $277 \pm 15$  Ma found for the oldest concordant zircon from this sample is the best estimate for the deposition age of this volcanic ash bed.

The mean  $\varepsilon\text{Hf}(t)$  calculated for the zircon grains from the three dated volcanic ash beds Lat20-1, Gal21-7 and Cam20-3 provides chondritic to subchondritic values of  $0.1 \pm 0.2$ ;  $-1.2 \pm 0.4$  and  $-3.6 \pm 0.5$ , respectively. The corresponding Hf model ages of 1.3–1.5 Ga represent an average of the sources involved in magma genesis or assimilated during the travel path upward to the surface of the magmas. In any case, this indicates a significant degree of recycling of Proterozoic or older material, which is also consistent with the occurrence (in the three volcanic levels) of zircon grains with apparent ages ranging from the Archean to the Neoproterozoic. It is however difficult to evaluate whether the Hf isotope signature of the analysed zircon grains reflects either a source signature or an open system evolution, such as assimilation of an older crust by juvenile, mantle-derived, magmas. Clarification of this point is key to the interpretation of the geochemical data, as it could indicate crustal reworking processes, or new crustal growth by addition of material issued from the mantle during the post-collisional Variscan period. Although sampled at different stratigraphical levels, samples Gal21-7 and Cam20-3 belong to the same F4/F5 formation and display remarkably similar U–Pb ages (278.4 and 278.7 Ma, respectively) and trace- and major-element chemistry. Both samples display subchondritic, but substantially different, Hf isotope signatures ( $\varepsilon\text{Hf} = -1.2 \pm 0.4$  and  $-3.6 \pm 0.5$  respectively). This difference indicates that magma genesis involved partial melting of a compositionally heterogeneous crustal section. The mean age for this crustal section is estimated between 1.3–1.6 Ga, assuming felsic precursors (with a  $^{176}\text{Lu}/^{177}\text{Hf}$  ratio of 0.015), or 1.6–2.0 Ga, assuming mafic precursors (with a  $^{176}\text{Lu}/^{177}\text{Hf}$  ratio of 0.021). Sample Lat20-1 yields a chondritic value that can be explained

in two ways. The first is a mixing (at *c.* 280 Ma) between a suprachondritic mantle-derived magma and subchondritic Paleoproterozoic or older crustal sources in proportions that coincidentally produced a  $\varepsilon\text{Hf}$  chondritic value. An alternative possibility is a remelting (at *c.* 280 Ma) of a 1.3 Ga old or 1.6 Ga old Paleoproterozoic source, which would have evolved with a calculated  $^{176}\text{Lu}/^{177}\text{Hf}$  ratio of, respectively, 0.015 assuming a felsic precursor, or a ratio of 0.021, typical of the time-integrated evolution of a mafic (lower) crust (Figure 9). It is worth noting that the vertical scattering observed for all analyses in Figure 9 (from 0.8 to  $-4.8$ ) may reflect such a mixing trend between mantle- and crustally-derived components. Whichever hypothesis is retained, it requires a heat source that can be found in mantle-derived magmas present at the base of the continental crust, as mentioned in many previously published studies [e.g. Breiterkruz and Kennedy, 1999]. Therefore, although our results indicate intra-crustal remelting and recycling of an old Paleoproterozoic to Archean basement, the addition of juvenile magmas triggering partial melting of the lower crust or mixed with crustally-derived magmas cannot be ruled out.

Although this needs further investigation, the Hf analyses tend to indicate an increase of crustal input in the production of the magmas, with  $\varepsilon\text{Hf}$  chondritic values for the oldest sample (Lat20-1) becoming increasingly negative towards the top of the basin. Interestingly, there is also a correlation between  $\varepsilon\text{Hf}(t)$  and  $\text{Eu}/\text{Eu}^*$ , which may indicate that the magmas producing the stratigraphically most elevated volcanic ash beds Gal21-7 and Cam20-3 underwent fractional crystallization processes involving plagioclase, more pronounced than the other samples, and that they possibly had more time to interact with, and assimilate crustal material.

The first group of samples consists of trachyandesitic lavas, which are characterized by a greater HREE depletion and smaller  $\text{Eu}/\text{Eu}^*$  anomalies than the rhyodacitic samples of group 2 (including the dated samples Lat20-1, Gal21-7 and Cam21-3). The greater HREE depletion of group 1 samples may indicate that the magmas were generated at a greater depth than samples from group 2. Lastly, the identification of Neoproterozoic to Archean zircon grains in the volcanic ashes substantiates the occurrence of a complex and old basement both underneath and alongside the basin.

The different geochemical signatures of the two groups mark a significant change in the petrological processes producing the magmas, especially an evolution of the main magmatic sources involved, as the geodynamical conditions evolved from a late- to a post-orogenic setting with time. The “Within Plate”- versus “Active Margin”-like signatures, coupled with our Hf data interpretations in the younger group, reflect that the crustal contribution increased as time proceeded. In any late- to post-orogenic setting, this has to be controlled by substantial modifications of the geothermal gradient, and a significant increase of the heat flux, which can hardly be conceived without a simultaneous increase of the production of mantle melts triggering crustal melting. Because the production of mantle magmas at high rates may induce significant crustal melting, it is likely that from the base to the top of the sedimentary succession, the Saint-Affrique pyroclastic layers recorded the transition from a late-orogenic extension to a post-orogenic extension at much higher rates as the basin enlarged.

Our new constraints on the age and nature of the volcanism recorded in the sedimentary succession also questions the location of the emission centres of the volcanic ashes, in the absence of known volcanic edifices near the Saint-Affrique Basin, feature which is a recurrent issue in Western Europe Carboniferous and Permian continental basins [e.g. Koniger and Stollhofen, 2001, Pellenard *et al.*, 2017]. Explosive subaerial calc-alkaline volcanic activity with Permian ages is known in the Central Pyrenees (about 200 km from the Saint-Affrique Basin), where it is associated with high-intensity explosive magmatic eruptions of rhyodacitic to rhyolitic lavas and associated widespread pyroclastic flows and overriding ash clouds [Marti, 1996, Pereira *et al.*, 2014], and transported several hundreds of kilometres under the dominant wind. On the other side, Permian subaerial calc-alkaline volcanic episodes, including andesitic, dacitic and rhyolitic ignimbrite lavas are known in northwestern Corsica and Sardinia [Cabanis *et al.*, 1990, Timmerman, 2004, and references therein], and in the Esterel Massif [Zheng *et al.*, 1992, Nmila, 1995], and could also represent good candidates for the volcanic ash input. Nonetheless, the possible pyroclastic flow nature of the sampled layer from the *Dourdou* Fm (sample Lat20-1) suggests that edifices that were more proximal to the basin still

have to be identified.

## 5.2. Implications for the deposition of the Saint-Affrique Basin

The new radiochronological ages presented in this study refine the chronological setting of the Saint-Affrique Basin (Figure 11), the sedimentary successions of which were considered as deposited from the early to the middle Permian [Rolando *et al.*, 1988, Figures 2 and 11], and then during the early Permian only [Gand, 1993, Figures 2 and 11]. Our new ages encompass the Kungurian Stage (uppermost Cisuralian, Figure 11). The oldest age (Lat20-1,  $280.3 \pm 2.6$  Ma), i.e. in the lower part of the *Dourdou* Fm, is, within errors, very close to the lower limit of the Kungurian, given that the Artinskian–Kungurian boundary is set at  $283.5 \pm 0.6$  Ma [Cohen *et al.*, 2013, updated; Figure 11]. No age could be determined at the base of the sedimentary succession, but it is likely that Asselian to Sakmarian (lower Cisuralian) deposits are preserved.

The top of the sedimentary succession of the Saint-Affrique Basin is not dated, but considering the youngest age found in this study (Cam20-3,  $278.7 \pm 2.4$  Ma), located less than 100 m below the youngest preserved deposits, as well as the absence of significant erosional surfaces or discontinuity in the sedimentation above this volcanic level, it is highly probable that the top of the sedimentary succession was also deposited during the Kungurian, the upper limit of which is set at  $273.01 \pm 0.14$  Ma [Cohen *et al.*, 2013, updated].

The maximum duration of the sedimentary deposition between the stratigraphically lowest and highest dated volcanic ash beds levels, i.e. Lat20-1 ( $280.3 \pm 2.6$  Ma) and Cam20-3 ( $278.7 \pm 2.4$  Ma), is 6.6 Ma. During this timeframe, the sediment thickness estimated by coupling borehole data and spatial correlations [based on the 1/50,000 geological map of Guérangé-Lozes *et al.*, 1995] is about 1100 to 1500 m. Considering this maximum duration, the sedimentation rates (compacted sedimentary succession), appear to be low, ranging from 0.160 mm/yr to 0.230 mm/yr. It is worth noting the mean sedimentation rate estimated for other late-Carboniferous–early Permian basins presenting

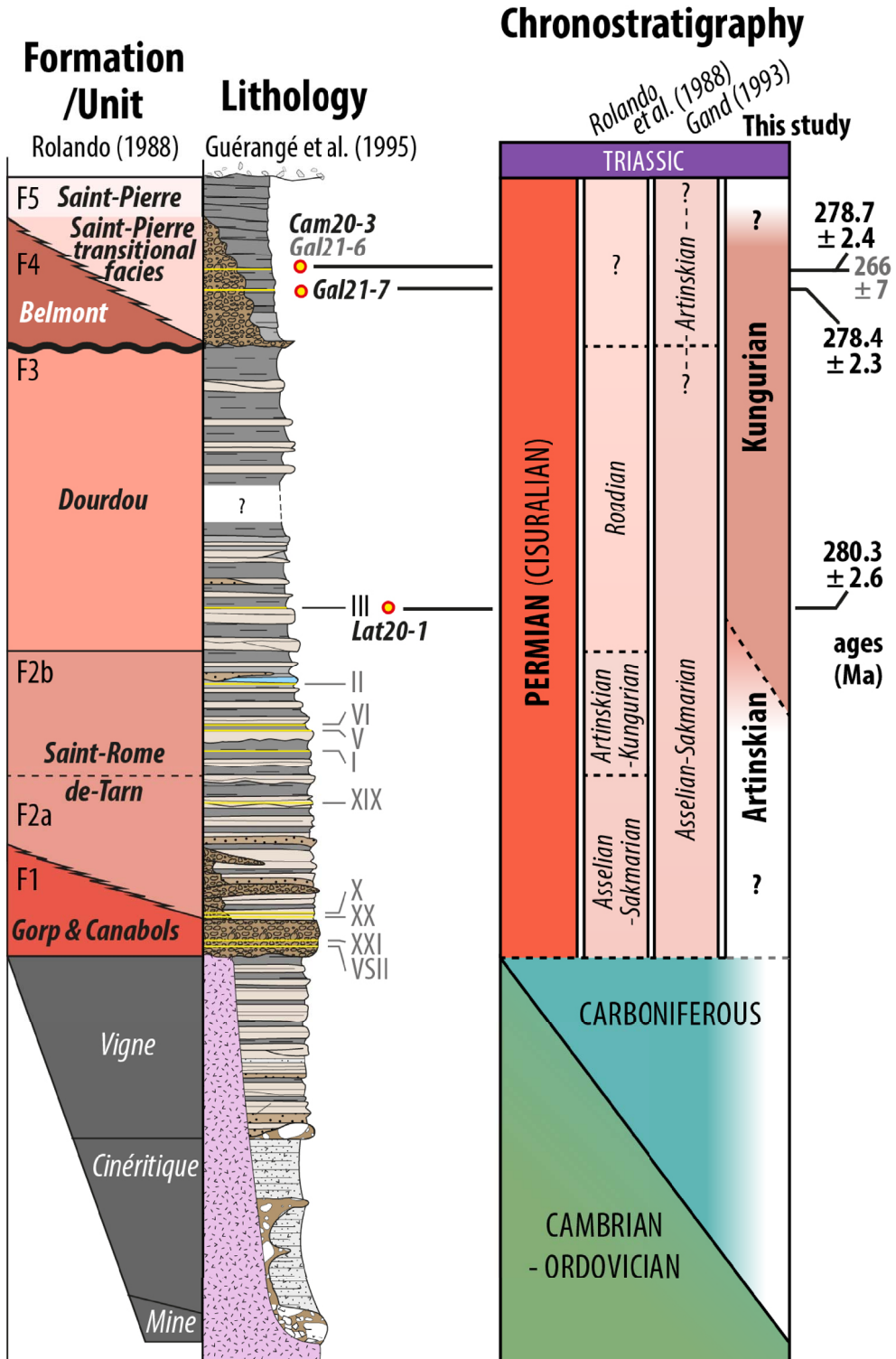


**Figure 11.** Refined chronostratigraphic setting for the Saint-Affrique Basin sedimentary succession based on the new ages obtained in this study.

a similar geological setting: in the northeastern Massif Central Autun Basin [Mercuzot, 2020], sedimentation rates based on precise radiometric ages were estimated at 0.45 mm/yr, taking the compacted sedimentary succession into account, and at 1.1 mm/yr when estimating a decompacted succession thickness. In the Saar-Nahe Basin (western Germany) the sedimentation rate is also higher, i.e. 0.3 mm/yr (compacted sedimentary succession). Some modern lacustrine systems, e.g. the Lake Titicaca (Altiplano, late-orogenic setting) and the North-American Great Lakes (Superior, Erie and Huron, glacial lakes) exhibit sedimentation rates between 0.1 and 7.4 mm/yr [Kemp and Harper, 1976, Kemp *et al.*, 1977, 1978, Durham and Joshi, 1980, Lojka *et al.*, 2009] that are consistent with our calculated rates. It also demonstrates that the sedimentation rates calculated in this study might be underestimated because of the lack of precise petrophysical and burial condition data. Consequently, the discontinuity between F3 and F4 fms (Figures 2 and 11) should not represent a substantial hiatus.

These new chronostratigraphical data clearly indicate the lack of the Middle (Guadalupian) and Upper (Lopingian) Permian deposits in the present-day sedimentary succession. Moreover, if we consider a middle-Anisian age for the basal Triassic sandstone deposits, as in the Lodève Basin [Lopez and Mader, 1985], the angular unconformity between the youngest Permian and the Triassic deposits represents a major hiatus of about 23 Myrs, during which the residual Variscan reliefs and the upper part of the Permian sedimentary succession of the Lodève and Saint-Affrique basins were eroded and peneplaned. In the Lodève Basin, the overall thickness of the eroded sedimentary succession between the top of the Permian deposits and the middle-Anisian unconformity is estimated at 1000 to 1500 m [Lopez *et al.*, 2008, Figure 2].

In Europe, increasing correlations are tentatively made between Carboniferous–Permian basins, based on both radiometric ages and biostratigraphic data [e.g. Schneider and Scholze, 2018, Pellenard *et al.*, 2017, Ducassou *et al.*, 2019, Schneider *et al.*, 2020]. The Lodève Basin is one of the most used basin to establish correlations in Western Europe, mostly because of its almost complete sedimentary succession from the late Carboniferous to the late Guadalupian [i.e. late middle Permian; Schneider

*et al.*, 2020]. However, the present re-evaluation of the ages of the Saint-Affrique Basin, located in the direct vicinity and formed in the same geodynamic setting, calls for new radiometric age constraints in the Lodève Basin.

## 6. Conclusion

Our study focuses on several volcanic ash beds encountered within the sedimentary successions of the Saint-Affrique Basin. Two different groups of volcanoclastic rocks are defined: (i) the first group, located at the base of the sedimentary succession and considered as Carboniferous in age, could not be dated due to a lack of volcanic zircon grains in the studied samples, and hence requires further analyses to refine the age of these ante-Artinskian deposits. These volcanoclastic beds include a significant terrigenous input and yield mostly trachytic to trachy-andesitic felsic compositions. They can be defined as calc-alkaline rocks that reproduce, in a late orogenic setting, a “Within Plate Volcanic Zone” signature; (ii) the second group consists of dacitic to rhyodacitic ash beds with a calc-alkaline affinity, and a geochemical signature resembling to that of “Active Continental Margin” rocks. Their deposition ages are younger than previously estimated, i.e. Kungurian instead of Artinskian.

The geochemical analyses (elemental and isotopic) of samples from both groups attest to a crustal recycling of older material (Proterozoic and older). This crustal component becomes more prominent toward the top of the Permian successions, possibly due to an increase of a mantle contribution triggering crustal melting. Overall, their petrological and geochemical features are compatible with volcanic activities that took place during late- to post-collisional regional extension. These types of volcanic centres are known during the late Carboniferous and Permian, both in the Central Pyrenees and in the Provence–Corsica–Esterel domain. The presence of these different volcanoclastic ash beds within the basin demonstrates the persistence and recurrence of the volcanic activity in the region during the Permian. Lastly, although preliminary, these new ages allow to calculate rather low minimum sedimentation rates (around 0.2 mm/yr) during the Kungurian in the Saint-Affrique Basin.

The dating the volcanic ash bed from the outcrop of Latour-sur-Sorgues (Lat20-1 sample, evidenced as a key-bed in 70's mining reports in drilled wells located along the southeastern border of the basin) would constitute a new robust anchor point to precisely correlate the sedimentary successions at basin-scale. Furthermore, several other volcanic ash beds, which unfortunately were not recognized in the field during this work, were also identified during the 70's at the same stratigraphical position on the different logs in the *Saint-Rome-de-Tarn* Fm (F2). Identifying these discrete volcanic levels in the *Saint-Rome-de-Tarn* Fm cropping out in the hanging wall of the southern bordering fault would make it easier to date the oldest Permian deposits of the basin.

While contributing to the refinement of the stratigraphic setting of the Saint-Affrique Basin, this study also demonstrates the need for additional precise dating in the neighbouring basins (e.g. Lodève Basin), as well as in other late Paleozoic basins from Western Europe related to the late Variscan dynamics. This would provide some important contributions for the recalibration of the Western Europe continental biostratigraphic scales. In addition, establishing correlations between these basins is paramount to better constrain the precise and accurate timing of their filling history, the relationships between sedimentation and tectonic and geodynamic processes, and to assess the various climate events that prevailed during the Permian in the Eastern Pangea intertropical domain.

### Conflicts of interest

Authors have no conflict of interest to declare.

### Acknowledgements

This study is dedicated to the memory of Jean-Louis Paquette who greatly contributed, among other things, to our understanding of the French Massif Central. Xavier Le Coz (Géosciences Rennes) is thanked for the making of the thin sections, and Cindy Maliverney (TSL) for sample preparations. Jean Poujol is thanked for his hospitality during the two sampling fieldtrips and Sara Mullin for correcting the English content. Finally, the authors want to thank J. Barbarand, V. Bosse and S. Duchêne for their insightful comments on the previous version of this manuscript.

### Supplementary data

Supporting information for this article is available on the journal's website under <https://doi.org/10.5802/crgeos.184> or from the author.

### References

- Beccaletto, L., Capar, L., Serrano, O., and Marc, S. (2015). Structural evolution and sedimentary record of the Stephano–Permian basins occurring beneath the Mesozoic sedimentary cover in the southwestern Paris basin (France). *Bull. Soc. Géol. Fr.*, 186, 429–450.
- Becq-Giraudon, J. F., Montenat, C., and Van Den Driessche, J. (1996). Hercynian high-altitude phenomena in the French Massif Central: tectonic implications. *Palaeogeogr. Palaeoclimatol. Palaeoecol.*, 122, 227–241.
- Blichert-Toft, J. (2008). The Hf composition of zircon reference material 91500. *Chem. Geol.*, 253(3/4), 252–257.
- Bourquin, S., Bercovici, A., López-Gómez, J., Diez, J. B., Broutin, J., Ronchi, A., Durand, M., Arche, A., Linol, B., and Amour, F. (2011). The Permian–Triassic transition and the beginning of the Mesozoic sedimentation at the Western peri-Tethyan domain scale: palaeogeographic maps and geodynamic implications. *Palaeogeogr. Palaeoclimatol. Palaeoecol.*, 299, 265–280.
- Bouvier, A., Vervoort, J. D., and Patchett, P. J. (2008). The Lu–Hf and Sm–Nd isotopic composition of CHUR: Constraints from unequilibrated chondrites and implications for the bulk composition of terrestrial planets. *Earth Planet. Sci. Lett.*, 273, 48–57.
- Breitkreuz, C. and Kennedy, A. (1999). Magmatic flare-up at the Carboniferous/Permian boundary in the NE German Basin revealed by SHRIMP Zircon Ages. *Tectonophysics*, 302, 307–326.
- Bruguier, O., Becq-Giraudon, J.-F., Champenois, M., Deloule, E., Ludden, J., and Mangin, D. (2003). Application of in situ zircon geochronology and accessory phase chemistry to constraining basin development during post-collisional extension: a case study from the French Massif Central. *Chem. Geol.*, 201, 319–336.
- Bruguier, O., Caby, R., Bosch, D., Ouzegane, K., Deloule, E., Dhuime, B., Bendaoud, A., and Kienast,

- J. R. (2020). A case study of in situ analyses (major and trace elements, U-Pb geochronology and Hf-O isotopes) of a zircon megacryst: implication for the evolution of the Egéré terrane (Central Hoggar, Tuareg Shield, Algeria). *Precambrian Res.*, 351, article no. 105966.
- Burg, J. P., Brun, J. P., and Van Den Driessche, J. (1990). Le sillon houiller du Massif Central français : faille de transfert pendant l'aminicissement crustal de la chaîne. *C. R. Acad. Sci. Paris*, 311, 147–152.
- Burg, J. P., Van Den Driessche, J., and Brun, J. P. (1994). Syn-to post-thickening extension: mode and consequences. *C. R. Acad. Sci. Paris*, 319, 1019–1032.
- Cabanis, B., Cochemé, J. J., Vellutini, P. J., Joron, J. L., and Treuil, M. (1990). Post-collisional Permian volcanism in northwestern Corsica: an asseement based on mineralogy and trace-element geochemistry. *J. Volcanol. Geotherm. Res.*, 44, 51–67.
- Carignan, J., Hild, P., Mevelle, G., Morel, J., and Yeghicheyann, D. (2001). Routine analyses of trace elements in geological samples using flow injection and low pressure on-line liquid chromatography coupled to ICP-MS: A study of geochemical reference materials BR, DR-N, UB-N, AN-G and GH. *Geostand. Newsl.*, 25, 187–198.
- Châteauneuf, J.-J. and Farjanel, G. (1989). Synthèse géologique des bassins permien français. In *Mémoires du Bureau de Recherches Géologiques et Minières*, volume 128, page 288. BRGM, Paris.
- Choulet, F., Faure, M., Fabbri, O., and Monié, P. (2012). Relationships between magmatism and extension along the Autun–La Serre fault system in the Variscan Belt of the eastern French Massif Central. *Int. J. Earth Sci.*, 101, 393–413.
- Cohen, K. M., Finney, S. C., Gibbard, P. L., and Fan, J.-X. (2013). The ICS International Chronostratigraphic Chart. *Episodes*, 36, 199–204. (updated).
- David, A. (1967). *Etude géologique du bassin permien de Belmont-sur-Rance (Aveyron) et ses minéralisations uranifères et cuprifères*. Thèse 3ème cycle, Université de Clermont-Ferrand. 96 pages.
- Dhuime, B., Hawkesworth, C., and Cawood, P. (2011). When continents formed. *Science*, 331, 154–155.
- Domeier, M. and Torsvik, T. H. (2014). Plate tectonics in the late Paleozoic. *Geosci. Front.*, 5(3), 303–350.
- Ducassou, C., Mercuzot, M., Bourquin, S., Rossignol, C., Beccaletto, L., Pierson-Wickmann, A. C., Pellenard, P., Poujol, M., and Hue, C. (2019). Sedimentology and U-Pb dating of Carboniferous to Permian continental series of the northern Massif Central (France): local palaeogeographic evolution and larger scale correlations. *Palaeogeogr. Palaeoclimatol. Palaeoecol.*, 533, article no. 109228.
- Durham, R. and Joshi, S. (1980). Recent sedimentation rates, 210Pb fluxes, and particle settling velocities in Lake Huron, Laurentian Great Lakes. *Chem. Geol.*, 31, 53–66.
- Faure, M. (1995). Late orogenic carboniferous extensions in the Variscan French Massif Central. *Tectonics*, 14, 132–153.
- Faure, M. and Becq-Giraudon, J. F. (1993). Sur la succession des épisodes extensifs au cours du désépaissement carbonifère du Massif Central français. *C. R. Acad. Sci. Paris*, 316, 967–973.
- Fisher, C. M., Hanchar, J. M., Samson, S. D., Dhuime, B., Blichert-Toft, J., Vervoort, J. D., and Lam, R. (2011). Synthetic zircon doped with hafnium and rare earth elements: A reference material for in situ hafnium isotope analysis. *Chem. Geol.*, 286, 32–47.
- Gand, G. (1993). La palichnofaune de vertébrés tétrapodes du bassin permien de Saint-Affrique (Aveyron) : comparaisons et conséquences stratigraphiques. *Géol. de la France*, 1, 41–56.
- Gand, G., Garric, J., Schneider, J., Sciau, J., and Walter, H. (1996). Biocénoses à méduses du permien français (bassin de Saint-Affrique, Massif Central). *Geobios*, 29/4, 379–400.
- Genna, A., Roig, J. Y., Debriette, P. J., and Bouchot, V. (1998). Le bassin houiller d'Argentat (Massif Central français), conséquence topographique d'un plissement de son substratum varisque. *C. R. Acad. Sci. Paris*, 327, 279–284.
- Goloubinoff, C. (1979). *Le permo-houiller du nord du bassin de St Affrique (Aveyron)*. Thèse de 3ème cycle, Université Paris-Sud. 143 pages.
- Guérangé-Lozes, J. and Alabouvette, B. (1999). *Carte Géologique de la France au 1/50 000 — feuille de Saint-Sernin-sur-Rance*. Bureau de Recherches Géologiques et Minières (BRGM), Orléans.
- Guérangé-Lozes, J., Burg, J. P., Vinchon, C., Alabouvette, B., Defaut, B., Astruc, J. G., Galharague, J., Leyreloup, A., Michard, A. G., Perrin, C., and Servelle, C. (1995). *Carte Géologique de la France au 1/50 000 — feuille de Réquista*. Bureau de Recherches Géologiques et Minières (BRGM), Orléans.
- Guérangé-Lozes, J. and Guérangé, B. (1991). *Carte Géologique de la France au 1/50 000 — feuille de*

- Camarès. Bureau de Recherches Géologiques et Minières (BRGM), Orléans.
- Hill, I. G., Worden, R. H., and Meighan, I. G. (2000). Yttrium: The immobility-mobility transition during basaltic weathering. *Geology*, 28, 923–926.
- Hübner, N., Körner, F., and Schneider, J. (2011). Tectonics, climate and facies of the Saint Affrique Basin and correlation with the Lodève Basin (Permian, Southern France). *Z. Dtsch. Ges. für Geowiss.*, 162(2), 157–170.
- Izart, A., Vaslet, D., Briand, C., Broutin, J., Coquel, R., Davydov, V., Donsimoni, M., Wartiti, M. E., Ensebaev, T., Geluk, M., Goreva, N., Gôrür, N., Iqbal, N., Joltaev, G., Kossovaya, O., Krainer, K., Laveine, J.-P., Makhlina, M., Maslo, A., Nemirovskaya, T., Kora, M., Kozitskaya, R., Massa, D., Mercier, D., Monod, O., Oplustil, S., Schneider, J., Schônlaub, H., Stschegolev, A., Süss, P., Vachard, D., Vai, G. B., Vozarova, A., Weissbrod, T., and Zdanowski, A. (1998). Stratigraphic correlations between the continental and marine Tethyan and Peri-Tethyan basins during the Late Carboniferous and the Early Permian. In Crasquin-Soleau, S., Izart, A., Vaslet, D., and De Wever, P., editors, *Peri-Tethys: Stratigraphic Correlations 2, Geodiversitas*, volume 20(4), pages 521–595. MNHN, Paris.
- Janousek, V., Farrow, C. M., and Erban, V. (2006). Interpretation of whole-rock geochemical data in igneous geochemistry: introducing Geochemical Data Toolkit (GCDKit). *J. Petrol.*, 47, 1255–1259.
- Jarvis, I. and Jarvis, K. E. (1985). Rare-earth element geochemistry of standard sediments: A study using inductively coupled plasma spectrometry. *Chem. Geol.*, 53, 335–344.
- Kemp, A., Dell, C., and Harper, N. (1978). Sedimentation rates and a sediment budget for Lake Superior. *J. Great Lakes Res.*, 4, 276–287.
- Kemp, A. and Harper, N. (1976). Sedimentation rates and a sediment budget for Lake Ontario. *J. Great Lakes Res.*, 2, 324–339.
- Kemp, A., MacInnis, G., and Harper, N. (1977). Sedimentation rates and a revised sediment budget for Lake Erie. *J. Great Lakes Res.*, 3, 221–233.
- Koniger, S. and Stollhofen, H. (2001). Environmental and tectonic controls on preservation potential of distal fallout ashes in fluvio-lacustrine settings: the Carboniferous-Permian Saar-Nahe Basin, south-western Germany. volume 30 of *Special Publication—International Association of Sedimentologists*, pages 263–284.
- Laversanne, J. (1976). *Sédimentation et minéralisation du Permien de Lodève*. Thèse doc/ing, Université d'Orsay. 300 pages.
- Le Maitre, R. W., Streckeisen, A., Zanettin, B., Le Bas, M. J., Bonin, B., and Bateman, P. (1989). Igneous rocks: a classification and glossary of terms. In *Recommendations of the International Union of Geological Sciences, Subcommittee on the Systematics of Igneous Rocks*, page 193. Blackwell, Oxford.
- Legrand, X. (1990). *Effets de la tectonique extensive en milieu continental. Le Bassin Permien de Saint Affrique*.
- Legrand, X., Soula, J.-C., and Rolando, J.-P. (1994). The Saint-Affrique Permian basin (southern France): an example of a roll-over controlled alluvial sedimentation during regional extensional tectonics. *Geodin. Acta*, 7(2), 103–120.
- Lojka, R., Drábková, J., Zajíc, J., Sykorová, I., Franc, J., Bláhová, A., and Grygar, T. (2009). Climate variability in the Stephanian B based on environmental record of the Mšec Lake deposits (Kladno-Rakovník Basin, Czech Republic). *Palaeogeogr. Palaeoclimatol. Palaeoecol.*, 280, 78–93.
- Lopez, M., Gand, G., Garric, J., and Körner, F. (2008). The playa environments of the Lodève Permian Basin (Languedoc, France). *J. Iber. Geol.*, 34, 29–56.
- Lopez, M. and Mader, D. (1985). Gravelly and sandy braidplain, evolving into floodplain and playa-lake deposition and vice versa, in the Bundsanstein facies sediments and marine incursions. In Mader, D., editor, *Triassic of the Lodève Region (Southern France)*, volume 4 of *Lecture Note in Earth Sciences*, pages 509–518. Heidelberg, Berlin.
- Lucas, S. G. and Shen, S.-Z. (2018). The Permian chronostratigraphic scale: history, status and prospectus. volume 450 of *Geol. Soc. Lond., Special Publications*, pages 21–50.
- Malavieille, J., Guihot, P., Costa, S., Lardeaux, J. M., and Gardien, V. (1990). Collapse of the thickened Variscan crust in the French Massif Central: Mont Pilat extensional shear zone and St. Etienne Late Carboniferous basin. *Tectonophysics*, 177, 139–149.
- Marti, J. (1996). Genesis of crystal-rich volcanoclastic facies in the Permian red beds of the Central Pyrenees (NE Spain). *Sediment. Geol.*, 106, 1–19.
- McDonough, W. F. and Sun, S. S. (1995). The composition of the Earth. *Chem. Geol.*, 120, 223–253.
- Ménard, G. and Molnar, P. (1988). Collapse of a Her-

- cynian Tibetan plateau into a late Palaeozoic European Basin and Range province. *Nature*, 334, 235–237.
- Mercuzot, M. (2020). *Reconstitutions paléoenvironnementales et paléoclimatiques en contexte tardi-orogénique : cas des bassins fini-carbonifères à permien du nord-est du Massif Central, France*. Thèse de 3ème cycle, Université de Rennes 1, France.
- Mercuzot, M., Bourquin, S., Beccaletto, L., Ducassou, C., Rubi, R., and Pellenard, P. (2021). Palaeoenvironmental reconstitutions at the Carboniferous–Permian transition south of the Paris Basin, France: implications on the stratigraphic evolution and basin geometry. *Int. J. Earth Sci.*, 110(1), 9–33.
- Mercuzot, M., Bourquin, S., Pellenard, P., Beccaletto, L., Schnyder, J., Baudin, F., Ducassou, C., Garel, S., and Gand, G. (2022). Reconsidering Carboniferous–Permian continental palaeoenvironments in eastern equatorial Pangea: facies and sequence stratigraphy investigations in the Autun Basin (France). *Int. J. Earth Sci.*, 111, 1663–1696.
- Mercuzot, M., Thomazo, T., Schnyder, J., Pellenard, P., Baudin, F., Pierson-Wickmann, A.-C., Sans-Jofre, P., Bourquin, S., Beccaletto, L., Santoni, A.-L., Gand, G., Buisson, M., Glé, L., Munier, T., Saloume, A., Boussaid, M., and Boucher, T. (2021). Carbon and nitrogen cycle dynamic in continental late-Carboniferous to early Permian basins of eastern Pangea (northeastern Massif Central, France). *Front. Earth Sci.*, 9, 1–24.
- Michel, L. A., Tabor, N. J., Montanez, I. P., Schmitz, M. D., and Davydov, V. I. (2015). Chronostratigraphy and paleoclimatology of the lodeve basin, France; evidence for a pantropical aridification event across the Carboniferous–Permian boundary. *Palaeogeogr. Palaeoclimatol. Palaeoecol.*, 430, 118–131.
- Morel, M. L. A., Nebel, O., Nebel-Jacobsen, Y. J., Miller, J. S., and Vroon, P. Z. (2008). Hafnium isotope characterization of the GJ-1 zircon reference material by solution and laser-ablation MC-ICPMS. *Chem. Geol.*, 255, 231–235.
- Nmila, A. (1995). *L’empreinte du volcanisme dans le remplissage permien du bassin de Lodève, étude pétrographique et géochimique, implication métallogénique*. Thèse de 3ème cycle, Université Pierre et Marie Curie, France.
- Nosenzo, F., Manzotti, P., Poujol, M., Ballèvre, M., and Langlade, J. (2022). A window into an older orogenic cycle: P–T conditions and timing of the pre-Alpine history of the Dora-Maira Massif (Western Alps). *J. Metamorph. Geol.*, 40/4, 789–821.
- Odin, B. and Conrad, G. (1987). Les cinérites, marqueurs aséquentiels au sein de la sédimentation permienne, continentale et rythmique, du bassin de Lodève (Hérault, France). *Ann. Soc. Géol. Belg.*, 110, 271–278.
- Paquette, J.-L., Piro, J.-L., Devidal, J.-L., Bosse, V., Didier, A., Sanac, S., and Abdelnous, Y. (2014). Sensitivity enhancement in LA-ICP-MS by N<sub>2</sub> addition to carrier gas: Application to radiometric dating of U-Th-bearing minerals. *Agilent ICP-MS J.*, pages 1–5.
- Patchett, J. P., Kouvo, O., Hedge, C. E., and Tatsumoto, M. (1981). Evolution of continental crust and mantle heterogeneity: evidence from Hf isotopes. *Contrib. Mineral. Petrol.*, 78, 279–297.
- Pellenard, P., Gand, G., Schmitz, M., Galtier, J., Broutin, J., and Stéyer, J. S. (2017). High-precision U-Pb zircon ages for explosive volcanism calibrating the NW European continental Autunian strato-type. *Gondwana Res.*, 51, 118–136.
- Pereira, M. F., Castro, A., Chichorro, M., Fernández, C., Díaz-Alvarado, J., Martí, J., and Rodríguez, C. (2014). Chronological link between deep-seated processes in magma chambers and eruptions: Permo-Carboniferous magmatism in the core of Pangaea (Southern Pyrenees). *Gondwana Res.*, 25, 290–308.
- Rolando, J.-P. (1988). *Sédimentologie et stratigraphie du bassin Permien de Saint-Affrique (Aveyron)*. Thèse de 3ème cycle, Université Paul Sabatier, Toulouse. 226 pages.
- Rolando, J.-P., Doubinger, J., Bourges, P., and Legrand, X. (1988). Identification de l’Autunien supérieur, du Saxonien et du Thuringien inférieur dans le bassin de Saint-Affrique (Aveyron, France). Corrélations séquentielles et chronostratigraphiques avec les bassins de Lodève (Hérault) et de Rodez (Aveyron). *C. R. Acad. Sci. Paris*, 307, 1459–1464.
- Rosignol, C., Hallot, E., Bourquin, S., Poujol, M., Jolivet, M., Pellenard, P., and Dabard, M. P. (2019). Using volcanoclastic rocks to constrain sedimentation ages: To what extent are volcanism and sedimentation synchronous? *Sedim. Geol.*, 381, 46–64.
- Schandl, E. S. and Gorton, M. P. (2002). Application of high field strength elements to discriminate tec-



- tonic settings in VMS environments. *Econ. Geol.*, 97, 629–642.
- Schneider, J. W., Lucas, S. G., Scholze, F., Voigt, S., Marchetti, L., Klein, H., Opluštil, S., Werneburg, R., Golubev, V. K., Barrick, J. E., Nemyrovska, T., Ronchi, A., Day, M. O., Silantiev, V. V., Rößler, R., Saber, H., Linnemann, U., Zharinova, V., and Shen, S. (2020). Late Paleozoic—early Mesozoic continental biostratigraphy—links to the Standard Global Chronostratigraphic Scale. *Palaeoworld*, 29, 186–238.
- Schneider, J. W. and Scholze, F. (2018). Late Pennsylvanian–Early triassic conchostracan biostratigraphy: a preliminary approach. volume 450 of *Geol. Soc. Lond., Special Publications*, pages 365–386.
- Scotese, C. R. and Langford, R. P. (1995). Pangea and the paleogeography of the Permian. In *The Permian of Northern Pangea*, pages 3–19. Springer, Berlin.
- Segal, I., Halicz, L., and Platzner, I. T. (2003). Accurate isotope ratio measurements of ytterbium by multiple collection inductively coupled plasma mass spectrometry applying erbium and hafnium in an improved double external normalization procedure. *J. Anal. Atom. Spectr.*, 18, 1217–1223.
- Sláma, J., Košler, J., Condon, D. J., Crowley, J. L., Gerdes, A., Hanchar, J. M., Horstwood, M. S. A., Morrish, G. A., Nasdalai, L., Norberg, N., Schaltegger, U., Schoene, B., Tubrett, M. N., and Whitehouse, M. J. (2008). Plesovice zircon – A new natural reference material for U–Pb and Hf isotopic microanalysis. *Chem. Geol.*, 249(1–2), 1–35.
- Söderlund, U., Patchett, P. J., Vervoort, J. D., and Isachsen, C. (2004). The  $^{176}\text{Lu}$  decay constant determined by Lu–Hf and U–Pb isotope systematics of Precambrian mafic intrusions. *Earth Planet. Sci. Lett.*, 219, 311–324.
- Stampfli, G. M., Hochard, C., Vérard, C., and Wilhem, C. (2013). The formation of Pangea. *Tectonophysics*, 593, 1–19.
- Stampfli, G. M. and Kozur, H. W. (2006). Europe from the Variscan to the Alpine cycles. *Mem.-Geol. Soc. Lond.*, 32, 57–82.
- Sun, S. S. and McDonough, W. F. (1989). Chemical and isotopic systematics of oceanic basalts: implications for mantle composition and processes. volume 42 of *Geol. Soc. Lond. Special Publications*, pages 313–345.
- Taylor, S. R. and McLennan, S. M. (1985). *The Continental Crust: its Composition and Evolution*. Blackwell, Oxford.
- Timmerman, M. J. (2004). Timing, geodynamic setting and character of Permo–Carboniferous magmatism in the foreland of the Variscan Orogen, NW Europe. In Wilson, M., Neumann, E.-R., Davies, G. R., Timmerman, M. J., Heeremans, M., and Larsen, B. T., editors, *Permo–Carboniferous Magmatism and Rifting in Europe*, volume 223 of *Geol. Soc. Lond., Special Publications*, pages 41–74.
- Vallé, B., Courel, L., and Gelard, J. P. (1988). Les marqueurs de la tectonique synsédimentaire et syndiagenétique dans le bassin stéphanien à régime cisailant de Blanzky-Montceau (Massif Central, France). *Bull. Soc. Géol. Fr.*, 4, 529–540.
- Van Den Driessche, J. and Brun, J. (1992). Structure and evolution of late Variscan extensional gneiss dome (Montagne Noire, southern Massif Central, France). *Geodin. Acta*, 5, 85–99.
- Van Den Driessche, J. and Brun, J. P. (1989). Un modèle cinématique de l’extension paléozoïque supérieur dans le Sud du Massif Central. *C. R. Acad. Sci. Paris*, 309, 1607–1613.
- Vermeesch, P. (2018). IsoplotR: A free and open toolbox for geochronology. *Geosci. Front.*, 9, 1479–1493.
- Vervoort, J. D., Patchett, P. J., Soderlund, U., and Baker, M. (2004). Isotopic composition of Yb and the determination of Lu concentrations and Lu/Hf by isotope dilution using MC-ICPMS. *Geochem. Geophys. Geosys.*, 5, 1–15.
- Winchester, J. A. and Floyd, P. A. (1977). Geochemical discrimination of different magma series and their differentiation products using immobile elements. *Chem. Geol.*, 20, 325–343.
- Witt, C., Rivadeneira, M., Poujol, M., Barba, D., Beida, D., Beseme, G., and Montenegro, G. (2017). Tracking ancient magmatism and Cenozoic topographic growth within the Northern Andes forearc: Constraints from detrital U–Pb zircon ages. *Geol. Soc. Am. Bull.*, 129(3–4), 415–428.
- Wood, D. A. (1980). The application of a ThHfTa diagram to problems of tectonomagmatic classification and to establishing the nature of crustal contamination of basaltic lavas of the British Tertiary Volcanic Province. *Earth Planet. Sci. Lett.*, 50, 11–30.
- Wray, D. S. (1999). Identification and long-range cor-

- relation of bentonites in Turonian-Coniacian (Upper Cretaceous) chalks of northwest Europe. *Geol. Mag.*, 136, 361–371.
- Wray, D. S. and Wood, C. J. (1998). Distinction between detrital and volcanogenic clay-rich beds in Turonian-Coniacian chalks of eastern England. *Proc. Yorkshire Geol. Soc.*, 52, 95–105.
- Zheng, J. S., Mermet, J.-F., Toutin-Morin, N., Hanes, J., Gondolo, A., Morin, R., and Féraud, G. (1992). Datation  $^{40}\text{Ar}$ - $^{39}\text{Ar}$  du magmatisme et de filons minéralisés permians en Provence orientale (France). *Geodin. Acta*, 5(3), 203–215.